AN ABSTRACT OF THE THESIS OF

Lawrence H. Sim for the degree of Master of Science in Geography presented on September 13, 2013.
Title: Blowout and Spill Occurrence Model

Abstract approved:

James J. Graham

To assist with risk-assessment with deepwater and ultra-deepwater prospects for offshore energy extraction as well as provide a useful tool for oil spill response, a spatially-explicit model was developed for comprehensive simulations of a blowout event from the wellhead to final fate and degradation. The Blowout and Spill Occurrence Model (BLOSOM) was created to handle deepwater jets and plumes, equations of state for crude oil mixtures and gases at great pressures, hydrate kinetics, non-surfacing plumes, and comprehensive weathering and degradation processes while maintaining the flexibility and adaptability required for risk assessment simulations.

BLOSOM is comprised of several components working in tandem to accurately simulate the various states and phases experienced by such a spill both through time and in light of the extreme pressures and physical conditions that a blowout event in great water depths will be

subjected to. These components include the crude oil model, the gas/hydrates model, the jet/plume model, the transport model, the weathering model, and the hydrodynamic handler.

Though their individual physics and algorithms works independently, they have been designed to coordinate and work in tandem to simulate the complexities and multi-phase physics of a blowout event. An integration of all separate parts, modifications to improve simulations in great water depths, attention to accurately handling conversions and transfers of data between models, a goal of adapting outputs for impact models, and an overarching design philosophy of flexibility for various locations and blowout conditions impart upon BLOSOM greater accuracy and ability to provide risk assessment capabilities.

# BLOWOUT AND SPILL OCCURRENCE MODEL

By

Lawrence H. Sim

A THESIS

submitted to

Oregon State University

In partial fulfillment of

the requirements for the

degree of

Master of Science

Presented on September 13, 2013

Commencement June 2014

Master of Science thesis of Lawrence H. Sim presented on the September 13, 2013.

APPROVED:

---

Major Professor, representing Geography

---

Dean of the College of Earth, Ocean, and Atmospheric Sciences

---

Dean of the Graduate School

I understand that my thesis will become part of the permanent collection of Oregon State University libraries. My signature below authorizes release of my thesis to any reader upon request.

---

Lawrence H. Sim, Author

# ACKNOWLEDGMENTS

I would like to acknowledge the works of the multitudes of researchers on whose enormous works this project builds upon. I would like to thank Kelly Rose and Jim Graham, who have supplied much advice and leadership on this project. The members of the graduate committee – Dr. Jim Graham, Dr. Julia Jones, Dr. Paul King, and Dr. Marta Torres – have provided the time and patience necessary for me to reach this point. Fellow members of the research group, past and current – Jim Eynard, Lucy Romeo, Jake Nelson, Jonathan Halama, Kaylyn van Ackeren, Corinne Disenhof, Jennifer Bauer, José Montero, McKenzie Moser, Chris Ringo, and others – have provided the support and resources for this project to come to fruition. I would like to thank the amazing assistance and helpfulness from the administration office without which I would never have managed graduate school. My mother, Young, has been integral for all the opportunities in my life, while my father has undoubtedly been the foundation for my curiosity in the sciences. My family, friends I have made here in Oregon, and old friends back home, who despite being too numerous to name individually, each deserve recognition for keeping my mental health intact. And to all the people I have met in my life who, for better or worse, have shaped me into who I am today.

# TABLE OF CONTENTS

# TABLE OF CONTENTS (Continued)

# LIST OF FIGURES

# LIST OF TABLES

# COMMON NOTATIONS AND SYMBOLS

$C_D$ = drag coefficient
$C_P$ = specific heat (J $kg^{-1}K^{-1}$)
$d$ = diameter (m)
$d_C$ = critical diameter (m)
$g$ = acceleration due to gravity (9.8 m $s^{-2}$)
$h$ = height or slick thickness (m)
$k_{jet}$ = jet coefficient
$M_{mol}$ = molar mass (g $mol^{-1}$)
$m$ = mass (kg)
$m_Q$ = mass entrained (kg)
$m_L$ = mass lost (kg)
$P$ = pressure (Pa)
$P_{atm}$ = atmospheric pressure (101,325 Pa)
$P_C$ = critical-pressure (Pa)
$P_r$ = reduced pressure $(P/P_C)$
$P_v$ = vapor-pressure (Pa)
$Q$ = entrained volume flux ($m^3$)
$Q_s$ = volume flux due to shear-entrainment ($m^3$)
$Q_f$ = volume flux due to forced-entrainment ($m^3$)
$R$ = gas constant (8.314 J $K^{-1}$ $mol^{-1}$)
$Re$ = Reynolds number
$r$ = radius (m)
$S$ = salinity (PSU)
$SG$ = specific gravity
$T$ = temperature (K)
$T_{bp}$ = boiling-point (K)
$T_{br}$ = boiling-point reduced
$T_C$ = critical-temperature (K)
$T_r$ = reduced temperature $(T/T_C)$
$T_{\circ C}$ = temperature (°C)
$t$ = timestep length (s)
$V$ = volume ($m^3$)
$V_{mol}$ = molar volume ($cm^3$ $mol^{-1}$ or $kg^3$ $kmol^{-1}$)
$v$ = velocity (m $s^{-1}$)
$v_t$ = terminal buoyant velocity (m $s^{-1}$)
$v_x$ = x-axis velocity (m $s^{-1}$)
$v_y$ = y-axis velocity (m $s^{-1}$)
$v_z$ = z-axis velocity (m $s^{-1}$)
$x$ = x-position (m)
$Y$ = fractional water-content
$y$ = y-position (m)
$Z$ = compressibility factor
$z$ = z-position/depth (m)
$\Delta\rho$ = density deficit (kg $m^{-3}$)
$\delta$ = droplet-size/diameter (m)
$\rho$ = density (kg $m^{-3}$)
$\Phi$ = elevation angle (radians)
$\theta$ = azimuth angle (radians)
$\nu$ = kinematic viscosity ($m^2$ $s^{-1}$)
$\sigma$ = interfacial tension (N $m^{-1}$)
$\mu$ = dynamic viscosity (Pa $s^{-1}$)

## COMMON SUBSCRIPTS

0 = initial conditions at blowout source
$a$ = ambient
$c$ = currents
$C$ = critical point
$k$ = *k*-th timestep
$pc$ = pseudocritical
$pr$ = pseudo-reduced
$pw$ = pure water
$r$ = reduced
$Q$ = entrained
$w$ = winds

## INTRODUCTION

The Macondo Blowout (also referred to as the Deepwater Horizon Oil Spill) introduced a complexity to oil spills that in many respects, response efforts were unaware of and unprepared for (Deepwater Horizon Study Group 2011). While a major offshore blowout had occurred at least once before in 1979 during the Ixtoc I oil spill (Jernelöv and Lindén 1981), the dynamics of a deepwater blowout were still not well understood. Besides the difficulty in responding to the spill, the event was complicated by the nature of non-surfacing oil plumes and the behaviors of natural gases at great depths, which deviate from the natural gas laws and for methane and ethane can form into hydrates at depths below 1000m (Yapa et al. 2001).

At the blowout source, the blowout releases a mixture of crude, gases, and water as a buoyant jet as depicted in Figure 1. Driven by its own buoyancy and momentum, the jet will drive upwards. However, as the jet rises, it will lose buoyancy and momentum as it entrains the ambient water, increasing its mass and volume with the exception of the gas bubbles, which will increase in buoyancy as the pressure drops. Due to both the natural difference in buoyancy and change in buoyancy between the gaseous and liquid parts of the jet/plume, the gas bubbles may separate in strong cross-flow conditions. In deepwater, high pressures and low temperatures may also spur the formation of hydrates, ice-like structures formed from water and natural gas. As the plume rises, the hydrates may then decompose into gas and water again. Both of these processes may affect the buoyancy of the jet/plume.

Once reaching some terminal-level, jet/plume-like behavior will cease and the spill will act more as a droplet cloud. At this stage, the jet/plume no longer acts as a singular unit and instead,

driven by individual buoyancies of oil droplets, will scatter and float to the surface. Some droplets however, may remain trapped below the surface. While the oil may be lighter the ambient seawater, this may be due to vertical turbulence, droplet-sizes, and/or a distinct stratification layer in the water column (Adalsteinsson et al. 2011). Besides being difficult to monitor, subsurface plumes do not undergo as significant of weathering and degradation as surfaced oil, and if eventually sinking, may present long-term consequences to the environment and benthic organisms. During the Deepwater Horizon Spill, a subsurface plume approximately 1000 meters below the ocean surface was detected, possibly exacerbated by the use of dispersants at the well-head with little detected microbial activity suggesting a slow biodegradation (Camilli et al. 2010).

In the mid-nineties, spill models were estimated at over 50, however most were focused on surface spills, rarely taking into account oil movement at depths (American Society of Civil Engineers 1996). Today, the number has grown tremendously, and more models factor in the 3-dimensional movement of hydrocarbons (Reed et al. 1999). It is an exhaustively researched field, yet one where many areas for improvement remain. Emulsification proves difficult to find an analytical solution for, while evaporation is a complex modeling problem for crude oils that contain a mixture of many different hydrocarbon compounds - though one that stands to benefit greatly from increased computational abilities (Reed et al. 1999). Longer term phenomena like biodegradation, photolysis, and sedimentation were somewhat ignored by many models since they focused on smaller, shorter-term spills, but necessitate further study in light of larger, long-term spills that through hopefully rare, do occur.

Research in blowout spill modeling has seen the emergence of jet/plume models such as the Clarkson Deepwater Oil and Gas Blowout Model (CDOG) (Zheng et al. 2002) and DEEPBLOW (Johansen 2000), borrowing heavily from the works of early sewage outfall modeling while innovating algorithms more suited to oil and gas blowouts. The original buoyant jet model by Lee and Cheung (1991) still forms the basis of most jet/plume models today, introducing the concept of Lagrangian control-volume analysis to blowout simulations. Yapa and Zheng (1997) improved upon this by integrating gas/bubble cores in the plume simulations. Johansen (2000) added gas/plume separation for sharply bending plumes and Yapa et al. (2001) followed shortly thereafter with methane hydrate formation.

The distributions of droplet sizes and their role in plume dynamics remain somewhat elusive. Jet/plume models tend to cease at the end of the momentum-dominated, jet-phase of the plume, typically for transfer to a particles-based predictive, transport model, still often far from the surface. Little has been written thus far on the methods of converting control-volumes to particles or how well to simulate the intermediate field when transferring between two very different types of models.

The Macondo Blowout exposed the lack in our understanding of deepwater spill dynamics and consequently these questions become extremely pertinent. If there were large, subsurface plumes as suggested by the observations of Camilli et al. (2010) and swaths of the seafloor can be covered with oil, impacts to the ecosystem could be much longer and more severe than originally expected. According to the Bureau of Safety and Environmental Enforcement (BSEE), there currently exists 125 active or leased fields in Gulf of Mexico considered ultra-deepwater (water-depth >5,000ft or roughly 1,500m) with the deepest at 9,436ft (roughly 2,876m), and the

race to tap ultra-deepwater prospects continues to accelerate with 20 prospective ultra-deepwater leases targeted as of August 2013.[1]

In light of this necessity, a multi-component modeling framework for simulating deepwater and ultra-deepwater blowouts was designed, incorporating recent advances in oil spill and blowout research into a single modeling package with overarching goals of maximizing utility to toxicity and impacts modeling in mind. The Blowout and Spill Occurrence Model (BLOSOM) has been developed to simulate such events, implementing physics suitable for high pressures, gas/hydrates chemistry, and long-term weathering and degradation processes, while meeting the necessary outputs criteria for potential impacts modeling and the flexibility for risk assessment modeling. An overview of the major components and their interactions may be seen in Figure 2.

The Jet/Plume Model handles the initial, near-field phases after a blowout, simulating the buoyant jet moving through the water-column until reaching a neutral buoyancy level. Here crude oils, gases, and entrained water are all modeled together and accuracy for high pressure conditions ensured. Droplet size distributions and terminal buoyant velocities are calculated to ensure accurate buoyancy behavior. Under high pressures and low temperatures, gas hydrates, an ice-like formation of gas and water, may also form and decompose, changing the physical properties of the plume (Yapa et al. 2001). The gases and hydrates may also separate from the

[1] Bureau of Safety and Environmental Enforcement (BSEE) (2013). "Deepwater Natural Gas and Oil Qualified Fields." <http://data.bsee.gov/homepg/data_center/other/tables/deeptbl2.asp> (14 August 2013).

plume under strong cross-currents due to the slip-velocity between the liquid and gas portions of the plume (Yapa et al. 2001).

The Crude Oil Model and Gas/Hydrates Model handles equations of state for crudes and gases accurate to such conditions as found on the ocean floor. The Gas/Hydrates Model also models hydrate formation and decomposition, slip-velocity from the plume, and some gas dissolution. The Crude Oil Model allows for the interpolation and approximation of various physical and chemical properties from relatively easily-obtained data, allowing for the adaptability to model any crude, either from real assay data or conjured from best estimates of reservoir composition.

A conversion model allows for the transfer of different modeling approaches between the Jet/Plume and Transport Models with minimum uncertainty, taking into account to distribution of different droplet sizes by volume fraction so as to account for separation portions of the plume splitting off in different layers due to different in terminal buoyant velocity. Once in the Transport Model, the crudes can then be handled as droplet clouds or portions of the surface slick, which undergo movement from advection by winds, waves, and currents, as well as turbulent diffusion.

A Weathering Model, in coordination with the Crude Oil Model, monitors the changes of the crude oil's physical and chemical properties through time from a variety of weathering process. A surfaced slick will spread laterally and thin; have droplets dispersed into the water column by wave-action; mix with water and become emulsified; evaporate; and experience other degradation processes that slowly remove the crude from the environment (Reed et al. 1999). These processes, besides some being natural clean up mechanisms, change the properties of the

crude so as to accelerate some processes and hinder others, becoming more and more significant for larger, long-term spills.

The objective of this research is to accurately model the spatial-temporal dynamics of a deepwater well blowout and the resulting oil spill with results that could then be used to predict the resulting impacts on the surrounding area as well as give insight into the less visible and observable phenomena such as subsurface transport. To do so successfully, uncertainties in input parameters and sensitivity to them must be assessed given that applications for quick response and risk assessment may have significant deficiencies in the data concerning exact blowout parameters. By accounting for the complexities present in a deepwater or ultra-deepwater blowout event, BLOSOM may help provide some answers to some of the controversies and questions surrounding such a spill as in Macondo – particularly the dynamics of subsurface oil plumes. Both from simulation runs and the development of the model, questions of why subsurface plumes form and how significant a role they play in major blowout events may be clarified. If droplet-sizes are the major contributor to subsurface plumes, how sensitive are the formation of subsurface plumes to the gas-to-oil volume-ratio (GOR) and blowout diameter, the two major predictors of droplet-sizes in the current model?

## Tables & Figures

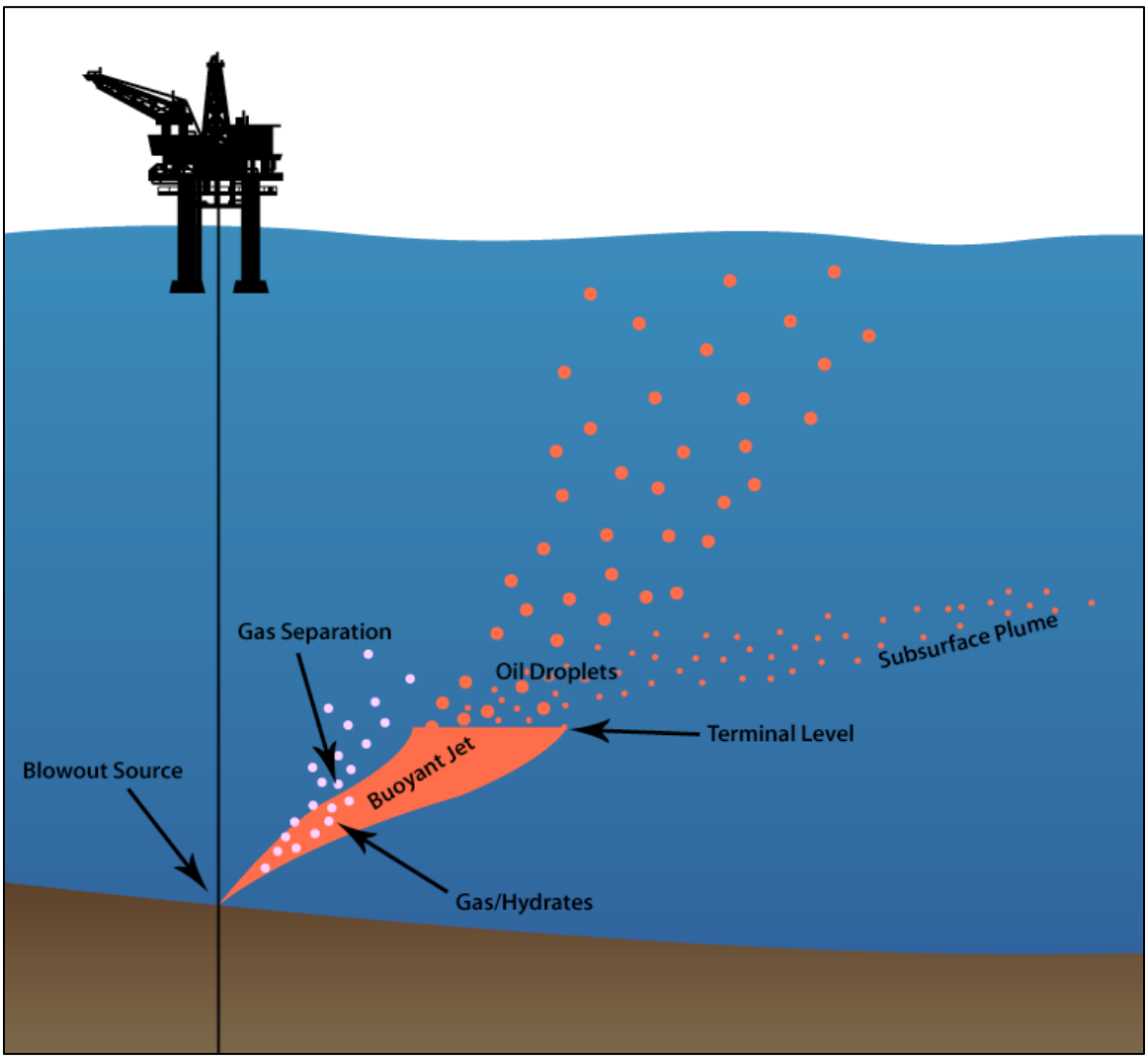


**Figure 1:** Generalized model of oil/gas blowout

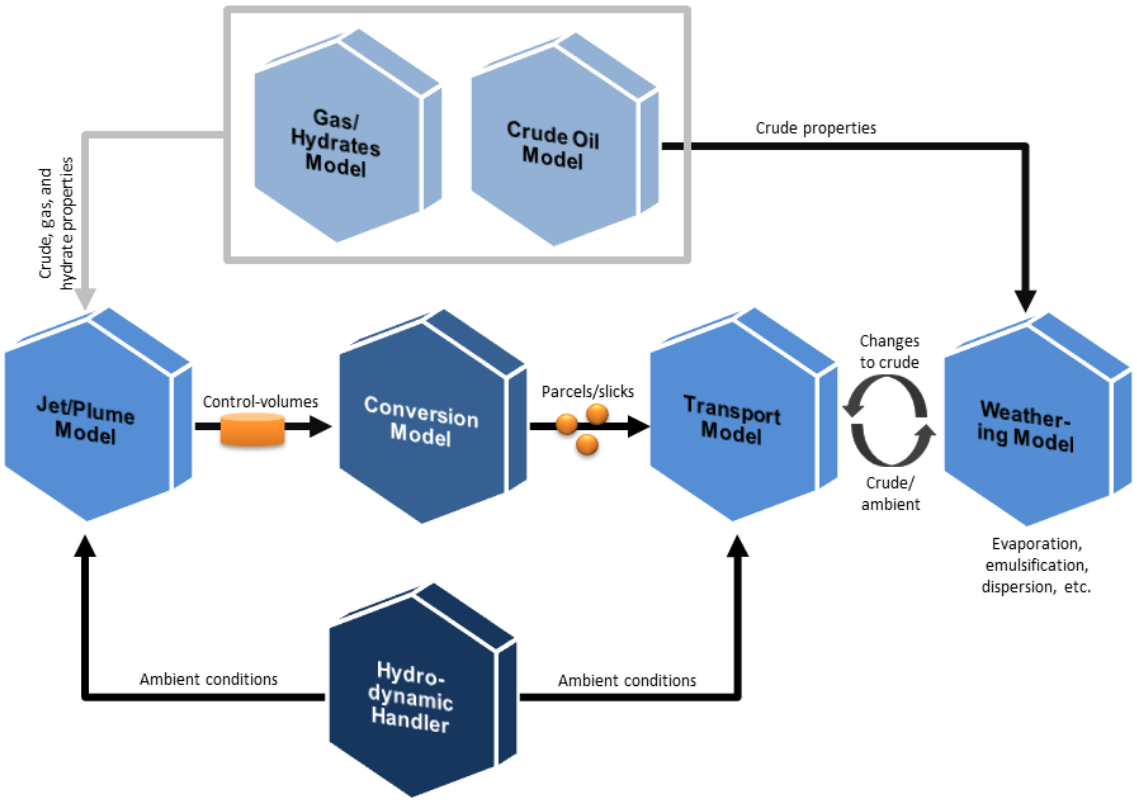


**Figure 2:** Overview of BLOSOM components

## THE JET/PLUME MODEL

At the source of a blowout, the oil rises as a buoyant jet with a high initial momentum, being expelled from the wellbore with great pressure. This jet can be multi-phase, containing crude oils and various gases. If conditions allow, clathrate hydrates of methane and ethane may also form and be present within the jet (Yapa et al. 2001). As the jet rises, water will be entrained into it, causing simultaneously the expansion and generally the slowing down of the jet (Lee and Cheung 1991). Eventually, what remains of the momentum will be less than that of the forces of buoyancy, at which point the system is no longer a jet but acting more as a plume or droplet cloud.

In the near-field phase, the Jet/Plume Model employs Lagrangian control-volume analysis as first proposed by Lee and Cheung (1991) to simulate blowouts as a conceptual volume of mixed hydrocarbons, gases, and entrained water, treating them all as a generalized, single entity. Such a concept can be visualized as taking cylindrical, cross-sectional slices of the jet/plume (Figure 3). The physics are largely controlled by momentum and buoyancy, and change is driven by entrainment of ambient water into the control-volume. As water is entrained, the volume and mass must be appropriately adjusted, but with this also comes a shift in density and momentum from the ambient, usually to slow down the jet.

The control-volumes are assumed to be non-interfering and cylindrical in shape. While the original control volumes in the JETLAG model bent to keep parallel with the trajectory of the plume (Lee and Cheung 1991), BLOSOM assumes the control-volume faces stay horizontal and instead the cylinders shear along their lengths to better simulate plumes dominated by

buoyancy and at depths in which cross-currents are unlikely to be very strong. Bending control-volumes were created with sewage outfalls in mind – usually oblique-facing pipes at shallow-depths. In large scales such as deepwater blowouts with mostly vertically oriented well heads, a shearing control-volume may better suit the simulations as the effects of the negative-volume and negative-buoyancy anomalies are eliminated. The effects of oil viscosity are ignored as it is assumed to be negated by the turbulent behavior of the plume.

## Governing Equations

The governing equations, except where otherwise noted, are unchanged from the originals given in Lee and Cheung (1991). Conservation of mass governs that the control volume's change in mass occurs only from a positive change due to entrainment (the addition of ambient water into the control volume) and some mass loss due to turbulence.

$$m_{k+1} = m_k + m_Q - m_L \tag{1}$$

Where $m_k$ denotes the mass at the current timestep, $m_Q$ represents the mass entrained, and $m_L$ the mass lost. Mass loss is due to turbulent diffusion and dissolution, but are ignored in the current version of the model as they are relatively insignificant (Yapa and Zheng 1997).

Conservation of momentum governs that the control volume's velocity changes due to the entrained momentum and acceleration due to buoyancy. Drag is ignored in the current model.

$$v_{k+1}^{0} = \frac{m_k v_k + m_Q v_a}{m_{k+1}} + \frac{\Delta\rho}{\rho_k} g t \boldsymbol{k} \tag{2a}$$

$$v_{k+1} = v_{k+1}^{0} + \left(1 - k_{jet}^{2}\right) a (v_a + v_T \boldsymbol{k} - v_{k+1}^{0}) \tag{2b}$$

Where $v$ is the velocity vector in some axis direction; $v_a$ is the velocity of the ambient fluid in that direction; $\rho$ is density and $\Delta\rho$ the density deficit, or the difference between the ambient and the control volume; $g$ is acceleration due to gravity; $t$ is the length of the timestep; and $\boldsymbol{k}$ is a unit vector in the upwards direction – that is, buoyancy is only a factor in the z-axis and ignored in x or y-axis calculations.

Equation 2b is a correction in which the jet coefficient $k_{jet}$ (to be explained later) is used to adjust the previously calculated velocity towards the ambient velocity and, if in the upwards the direction, the terminal droplet buoyancy ($v_t$) calculated for the maximum droplet size. The advection coefficient ($a$) is by default set to 1.0.

Conservation of heat controls changes in temperature using heat energy derived from the mass and specific heat of the present mixture of crudes, gases, and the entrained water. Specific heats are calculated in the crude oil, gas/hydrate, and hydrodynamic models. Heat diffusivity may be ignored as it was proven to be insignificant through validation testing. Salinity is calculated in a similar fashion by comparing the new salt content by the new total mass but only for the entrained water – salinity is assumed to not affect the gases or liquid crude.

$$I_{k+1}^{0} = \frac{(m_k - m_L) I_k + m_Q I_a}{m_{k+1}} \tag{3a}$$

$$I_{k+1} = I^0_{k+1} + (1 - k^2_{jet})a(I_a - I^0_{k+1}) \quad (3b)$$

Where '$I$' can represent a scalar value such as specific heat or salinity, and $I_a$ the corresponding value for the ambient. Likewise, the final heat and salinity are adjusted with the jet-coefficient in the same way as the velocity.

## Control-Volume Geometry

The height of the control volume is calculated from the previous displacement length as a ratio of the change in velocity. As the jet-phase reaches a neutral buoyancy level, the control-volume tends to exaggerate the effect of thinning and spreading out, thus as the control-volume begins to act more like a plume, height is assumed to not change, represented by the $k_{jet}$ coefficient in Equation 4b regulating the change in height. The radius is simply calculated from rearranging the formula for the volume of a cylinder using the given height, mass, and density.

$$h_{k+1} = h_k + \Delta h \quad (4a)$$

$$\Delta h = k_{jet}(V_{k+1} t \sin \Phi - h_k) \quad (4b)$$

$$r_{k+1} = \sqrt{\frac{m_{k+1}}{\rho_{k+1} \pi h_{k+1}}} \quad (4c)$$

Where $\Phi$ represents the velocity vector's elevation (angle from vertical) and $k_{jet}$ represents a jet-coefficient that will be explained later. Equation 4b corrects for sudden expansions in the plume when slowing down that often exaggerate spreading as the plume nears the terminal level.

## Entrainment

Lee and Cheung (1991) modeled the dynamics of a buoyant plume through shear and forced entrainment. The first is due to the boundary conditions of the control-volume element and the ambient fluid, which occurs regardless of ambient currents. The second is due to cross-flow conditions – i.e. ambient currents directly forcing entrainment into the control-volume.

The volume flux from sheer entrainment is calculated from the surface area of the control volume's sides, the difference between the velocity of the control-volume from the ambient's projected into the same direction, and a shear entrainment coefficient ($\alpha$) based on the Froude number ($F$), a number that is used to characterize the resistance of an object moving through water. The equations as adopted from Schatzmann (1979) by Lee and Cheung (1991) are below.

$$Q_s = 2\pi r h \alpha v' \cdot t \tag{5}$$

$$\alpha = \sqrt{2}\frac{0.057 + \frac{0.554 \sin \Phi}{F^2}}{1 + 5\frac{V_a'}{V'}} v' \tag{6}$$

$$F = E\frac{v'}{\sqrt{g\frac{\Delta\rho}{\rho}r}} \tag{7}$$

Where $Q_s$ is the volume flux entrained ($m^3$) due to sheer entrainment; $v'$ represents the absolute value of the difference between the control-volume's velocity and the ambient velocity projected into the control-volume velocity vector ($v_a'$); $E$ is a proportionality constant in the model assumed to be 2.0 (Yapa and Zheng 1997); and $t$ is the timestep in seconds.

The volume flux from forced entrainment is calculated as the apparent surface area of the sides of the control-volume element to the ambient current, expanded by the difference between the velocity and ambient velocity in that direction.

$$Q_{fx} = |v_x - v_{a,x}| \cdot 2rh \cdot t \tag{8a}$$

$$Q_{fy} = |v_y - v_{a,y}| \cdot 2rh \cdot t \tag{8b}$$

$$Q_{fz} = |v_z - v_{a,z}| \cdot 2rv\cos(\Phi) \cdot t \tag{8c}$$

Due to the use of the shearing control-volumes, these equations are modified from the original equations meant for bending control-volumes given in Lee and Cheung (1991).

Theoretically, the total entrained mass equals the sum of the volume-fluxes multiplied by the ambient density, meaning the entire volume-fluxes are used. However, full entrainment is unlikely, especially as the jet becomes less momentum-dominated, and BLOSOM uses a jet-coefficient $(k_{jet})$ to regulate entrainment and how the control-volume is behaving. Thus the total mass entrained is as follows.

$$M_Q = k_{jet}\rho_a(Q_f + Q_s) \tag{9}$$

## Jet Coefficient

Issues in some of the basic equations and a lack of corrections to a less turbulence-dominated system in the intermediate phase call for the use of a moderating algorithm that can help to blend the transition away from the momentum-dominated jet to physics closer to those used by

the transport model. A jet-coefficient has thus been designed to attempt to monitor the state of the control-volume from momentum-dominated jet to buoyancy-dominated plume and adjust the physics as necessary.

The jet-coefficient ($k_{jet}$) ranges from 0 (acting more as a cloud of individual droplets driven by buoyancy) to 1 (acting completely as a momentum-dominated jet with full entrainment). It is based on the difference in velocity from the ambient plus the terminal buoyant velocity.

$$k_{jet} = \tanh(\omega\pi|v - v'_{a+t}|) \tag{10}$$

Where $v$ is the magnitude of the velocity; $V'_{a+t}$ is the magnitude of the ambient plus terminal buoyant velocity projected onto $v$; and the coefficient $\omega$ is some user-defined parameter that adjusts the position and shape of the curve. For simulations in this paper, the default value of 5.0 was used. The calculations for terminal buoyant velocity are explained in the next section.

As the plume is less momentum dominated entrainment plays less of a role in the physical changes of the plume, the plume instead acting as a collection of buoyancy-driven droplets than a momentum-dominated jet. However, if the velocity difference was to increase (for example, a plume entering a layer of greater ambient currents), entrainment resumes a growing role again until the velocities are roughly even. When there is little excess momentum from the ambient and buoyant velocity, the jet-coefficient should reach zero or near to resulting in little to minimum entrainment. The shape should remain relatively constant due to minimal change in mass, and the velocity is controlled by advection and buoyant terminal velocity. Should the plume enter a strong cross-flow or stronger density difference, increasing the terminal buoyant velocity, the jet-coefficient may rise again, reintroducing entrainment into the system.

## Droplet Sizes and Terminal Buoyant Velocity

One of the major drivers of non-surfacing plumes is the distribution of droplet-sizes, as most crudes are less dense than seawater, even in their heavier components. Droplet sizes are proportional to the terminal buoyant velocity, meaning that smaller droplet sizes rise more slowly and are more easily trapped by turbulence, much like denser dust particulates may be suspended by turbulence in the air.

The maximum droplet size is calculated using a formula based on the blowout diameter and the Weber number ($W$) (Rye et al. 1996), and distribution of droplet sizes is assumed to follow a Rosin-Rammler distribution as described by Johansen (2002). When in a control-volume, the maximum droplet-size is used for all calculations involving droplet-sizes (e.g. terminal buoyant velocity).

$$\delta_{max} = k d_0 W^{-0.6} \tag{11a}$$

$$W = v_0^2 d_0 \rho \sigma^{-1} \tag{11b}$$

$$V_\delta = 1 - \exp\left[-2.996\left(\frac{\delta}{\delta_{max}}\right)^N\right] \tag{12}$$

Where $\sigma$ is the interfacial-tension of the oil-water interface; $V_\delta$ is the volume-fraction of droplets of diameter $\delta$ or smaller; and $k$ and $N$ are coefficients based on the void ratio, but for the purposes of this model, adjusted into two regimes – one for each a high or low GOR (gas-to-oil volume ratio), with the break set at a GOR of 19. As suggested by Johansen (2002), $k$ is set to 20 for a low GOR and 4 for a high GOR, and $N$ is set to 1.6 for a low GOR and 2.5 for a high GOR.

Likewise the interfacial tension for the mixed oil and gas plume is set to 0.03 N/m for a low GOR and 0.005 for a high GOR. The density $(\rho)$ is for the background fluid, which in the case of a low GOR is the ambient seawater, and in the case of a high GOR the gas.

To calculate the terminal droplet buoyancy $(\mathrm{v}_t)$, a three-phase approach for spherical, ellipsoidal, and spherical-cap droplet shapes (in order of increasing size regimes) is used as described in Zheng and Yapa (2000). This replaces the formally two-phase approach of spherical and ellipsoidal alone and provides greater accuracy for larger droplet sizes. The method described can be applied to any liquid and gas droplet/bubble and thus, the methods described can be applied both to the crude oil droplets and gas bubbles in the control-volume.

All droplets/bubbles with a diameter of 1mm or less are assumed to be spherical in shape and act like rigid particles. Their terminal velocity is obtained by using the equation below.

$$\mathrm{v}_t = \frac{\mathrm{Re} \cdot \mu}{\rho \mathrm{d}} \tag{13}$$

The Reynolds number ($Re$), a dimensionless ratio to characterize laminar or turbulent flow, is computed using the procedures described by Zheng and Yapa (2000).

$$\mathrm{N}_D = \frac{4\rho\Delta\rho g d^3}{3\mu^2} \tag{14}$$

$$\mathrm{W} = \log N_D \tag{15}$$

$$\begin{pmatrix} \mathrm{Re} = \frac{\mathrm{N}_D}{24} - 1.7569x10^{-4}N_D^2 + 6.9252x10^{-7}N_D^3 - 2.3027x10^{-10}N_D^4 & if\ \mathrm{N}_D \leq 73 \\ \log Re = -1.7095 + 1.33438W - 0.11591W^2 & if\ \mathrm{N}_D \leq 580 \\ \log Re = -1.81391 + 1.34671W - 0.12427W^2 + 0.006344W^3 & if\ \mathrm{N}_D > 580 \end{pmatrix} \quad (16)$$

In the ellipsoidal shape, defined as between 1mm diameter and the critical diameter $d_c$, the terminal velocity is determined by the Morton number ($M$) and the Eötvös number ($Eo$).

$$\mathrm{M} = \mathrm{g}\mu_{pw}^4 \left(\frac{\Delta\rho}{\rho^2}\right)\sigma \quad (17)$$

$$\mathrm{Eo} = \mathrm{g}\Delta\rho d^2/\sigma \quad (18)$$

$$\mathrm{H} = \frac{4}{3}EoM^{-0.149}\left(\frac{\mu}{\mu_{pw}}\right)^{-0.14} \quad (19)$$

$$\mathrm{J} = 0.94\mathrm{H}^{0.757}, \qquad if\ 2 < H \leq 59.3 \quad (20a)$$

$$\mathrm{J} = 3.42\mathrm{H}^{0.441}, \qquad if\ H > 59.3 \quad (20b)$$

$$\mathrm{v}_t = \frac{\mu}{\rho d}M^{-0.149}(J - 0.857) \quad (21)$$

If the droplet or bubble is larger than the critical diameter, it is assumed to be spherical-cap in shape and the terminal velocity governed almost solely by the densities of the droplet/bubble and the ambient fluid.

$$\mathrm{v}_t = 0.711\sqrt{gd\Delta\rho/\rho} \quad (22)$$

To obtain the critical diameter, an approximation method for where the terminal velocities for the ellipsoidal shape and spherical-cap shape coincide, as proposed by Zheng and Yapa (2000), is used.

$$\log d_c = \frac{b_1 - b_2}{0.5 - a} \tag{23a}$$

$$\mathrm{a} = \frac{y_2 - y_1}{x_1 - x_2} \tag{23b}$$

$$\mathrm{b}_1 = \log(0.711\sqrt{g\Delta\rho/\rho}) \tag{23c}$$

$$\mathrm{b}_2 = y_1 - ax_1 \tag{23d}$$

Where the set $(x_1, y_1)$ represents a point equivalent to $(\log d\,, \log v_t)$ when $H = 59.3$; and $(x_2, y_2)$ represents a point equivalent to $(\log d\,, \log v_t)$ when $d = 15mm$ in the ellipsoidal regime. As the critical diameter calculations do not need to be recalculated every timestep, one of a number of conditions must be met in the model to necessitate recalculating the critical diameter so as to maintain a high level of efficiency: either having not yet been calculated, surpassing a maximum timestep interval since last calculation, or significant changes in the viscosity or densities of either the droplet/bubble or ambient seawater. Additionally, the droplet diameter must be at least 10mm for either of the aforementioned conditions to trigger, as spherical-cap regimes do not often start in the smaller sizes, and if exceeding 25mm is assumed to be almost certainly in the spherical-cap regime and critical diameter calculations ignored.

## Gas/Bubble Separation

While the approach taken by using Lagrangian control-volumes simplifies the jet/plume in a control-volume containing the generalized mixture of crude, water, and gases in a relatively accurate fashion, it does make the assumption that the gas bubbles are rising at a similar rate or that ones that escape above are simply replaced by the control-volume below. However, gas bubbles will naturally rise faster than the liquid portions of the plume due to buoyancy, and in strong cross-currents, this creates an uneven horizontal displacement by depth, meaning that due to the slip-velocity between the gas bubbles and the liquid plume, gas bubbles will leak and peel off in strong cross-currents.

To calculate the slip velocity ($w_b$) a harmonic mean of two extreme slip velocity calculations are used as described in Johansen (2000). Further details are provided in the chapter concerning the Gas/Hydrates Model.

Assuming that the bubbles, though randomly dispersed within the control-volume, are relatively evenly dispersed, the model calculates the displacement of the control-volume and the equally-sized gas core extent. The volume of the gas-core no longer intersecting the control-volume is then multiplied by the original gas-fraction of the jet/plume to obtain the volume of gas to have separated from the plume. The process is adapted from the method described in Chen and Yapa (2004) and visualized by their diagram in Figure 4.

While methane may present a hazard to response if present in significant quantities at the surface, for purposes of this model, all gases are ignored once leaving the control-volume as in

deepwater and ultra-deepwater conditions it is assumed that most gases with undergo significant dissolution before surfacing.

## Additional Details

The timesteps are user-specified with a minimum and default timestep of 1 second. Up to 10 second timesteps have been tested with acceptable amounts of sensitivity/variance, but this will vary depending on the vertical velocity of the jet/plume and the rate of change of ambient conditions along the vertical. At each timestep, entrainment is calculated, after which density, volume, and velocities are recalculated. Density is calculated as the volume-averaged densities of non-miscible fluids. Between each step, these values are assumed constant, thus the model assumes a quasi-steady-state for the control-volumes as it moves through timesteps.

When the control-volume reaches the surface, crosses a neutral-density level, or falls below the terminal buoyant velocity, the model then logs the time at which the control-volume is no longer simulated by the jet/plume portion of the model and outputs to a layer ready for conversion in the next phase. For some simulations in this paper, the terminal level was logged but the model did not discard the control-volumes into an output layer to thoroughly test the plume model.

**Tables & Figures**

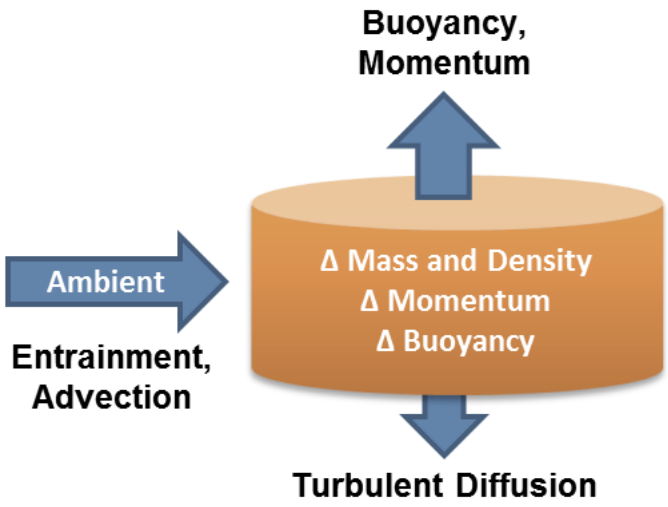


**Figure 3:** Generalized model of Lagrangian control-volume analysis

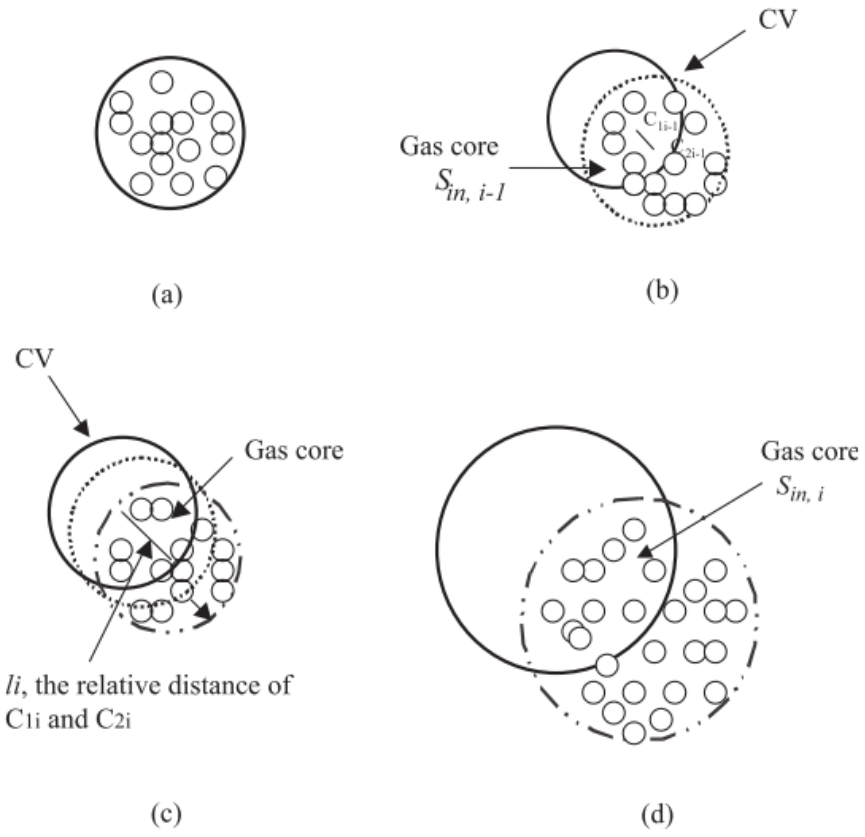


**Figure 4:** Gas separation of gas-core from control-volume (adapted from Chen and Yapa 2004)

## CRUDE OIL MODEL

Instead of a simplistic approach with crude properties handled within the Jet/Plume Model or the Transport Model, a separate entity was created for simulating the crude oil. In accordance with the overarching goal of providing detailed results for impact and toxicity modeling efforts, crude oils were not handled as a single entity with averaged physical properties, but split up into distillate fractions, each of which was independently monitored by the model. This provided a better fit with the pseudo-components approach to evaporation modeling (to be expounded on later) and allowed a more detailed picture of the exact composition of the crude in the output data. Simultaneously, the Crude Oil Model was designed to be flexible and adaptable to different crudes, allowing ease of importing different crude oil types from widely available assay data or even the customization of a user-defined crude.

Crude oil properties are loaded or defined as distillation cuts with associated volume or mass fractions, vapor temperatures, and specific gravities, for each of which the crude oil model approximates molecular mass, molar volume, and pseudocritical temperature and pressure. Molecular mass is estimated using the Kesler and Lee (1976) correlation given below.

$$\begin{aligned} M_{mol} = & -12272.6 + 9486.4 \cdot SG + (8.3741 - 5.99175SG)T_{bp} \\ & + (1 - 0.77084 \cdot SG - 0.02058 \cdot SG^2)\left(0.7465 - \frac{222.466}{T_{bp}}\right) \\ & + (1 - 0.77084 \cdot SG - 0.02058 \cdot SG^2)\Bigg(0.3228 \\ & - \frac{17.335}{T_{bp}}\Bigg)\frac{10^{12}}{T_{bp}^3} \end{aligned} \tag{24}$$

Where $SG$ is the specific gravity of the distillate cut and $T_{bp}$ the boiling point in Kelvin.

For the heaviest residuals, for which vapor temperatures are often not supplied, a 3rd order polynomial is fit to the existing distillation cut data of vapor temperature and specific gravity by volume fraction (e.g. $T_{BP} = f(V_f)$) to interpolate properties for the heaviest components which are often not measured.

If a simple, generalized crude with no specified distillate cuts data is given, only the API (American Petroleum Institute) gravity can be supplied. Average boiling point is estimated using the correlation from Shen et al. (1987) before correlating the other physical properties.

$$T_{bp} = 524.6 - 30.275\text{API} + 1.565\text{API}^2 - 0.03439\text{API}^3 + 0.002604\text{API}^4 \quad (25)$$

Molar volume is calculated using the Spencer-Danner approximation, which requires the critical temperature ($T_c$), critical pressure ($P_c$), and acentric factor ($\omega$) of the distillate cut. Kesler and Lee (1976) provided correlations for critical temperature and pressure, while the equations for the acentric factor was given by Chang et al. (2012).

$$T_c = 189.8 + 450.6SG + (0.4244 + 0.1174SG)T_{bp} + (0.1441 - 1.0069SG)10^5 T_{bp}^{-1} \quad (26a)$$

$$T_{br} = T_{bp}/T_c \quad (26b)$$

$$P_c = 5.689 - \frac{0.0566}{SG} - \left(0.43639 + \frac{4.1216}{SG} + \frac{0.21343}{SG^2}\right)10^{-3}T_{bp} \quad (27)$$

$$+\left(0.47579+\frac{1.182}{SG}+\frac{0.15302}{SG^2}\right)10^{-6}T_{bp}^2$$

$$-\left(2.4505+\frac{9.9099}{SG^2}\right)10^{-10}T_{bp}^3$$

$$\omega=\frac{-\ln\left(\frac{P_c}{1.01325}\right)-5.92714+\frac{6.09648}{T_{br}}+1.28862\ln(T_{br})-0.169347T_{br}^6}{15.2518-\frac{15.6875}{T_{br}}-13.4721\ln(T_{br})+0.43577T_{br}^6} \quad (28)$$

Equations for the density of a crude oil as a function of temperature and pressure are calculated using the Spencer-Danner equation for molar volume at saturated conditions and COSTALD (Corresponding States Liquid Density) method as described in Chang et al. (2012), where the density at temperature and a reference pressure ($\rho_0 = f(P_0)$) gathered from the Spencer-Danner method is used to predict the density at an elevated pressure.

$$V_{mol}^{SAT}=\left(\frac{RT_c}{P_c}\right)Z_{RA}^n \quad (29a)$$

$$Z_{RA}=0.29056-0.08775\omega \quad (29b)$$

$$n=1+(1-T_{br})^{2/7} \quad (29c)$$

$$\rho=\rho_0\left[1-C\ ln\left(\frac{B+P}{B+P_0}\right)\right]^{-1} \quad (30a)$$

$$\varepsilon=\exp(4.79594+0.250046\omega+1.14188\omega^2) \quad (30b)$$

$$B = P_c\left[-1 - 9.0702(1 - T_{br})^{1/3} + 62.45326(1 - T_{br})^{2/3} - 135.1102(1 - T_{br}) + \varepsilon(1 - T_{br})^{4/3}\right] \quad (30c)$$

$$C = 0.0861488 + 0.0344483\omega \quad (30d)$$

At each timestep, densities are calculated separately for each distillate cut, then mass-averaged, accounting for unequal degradation rates of separate distillate cut. If however, no degradation has occurred or a simplistic version of the crude without specified distillate cuts is used, for example during the near-field simulations of the jet/plume model, a more simplistic algorithm can be applied using the measured density and specific gravity of the entire crude.

For evaporation, vapor pressure $(P_V)$ of the crude plays a significant factor. Accordingly, vapor pressure is estimated using a simplified version of the Clausius-Clapeyron equation as described in Fingas (1995).

$$P_V = \frac{\mathrm{P}_{bp}}{\exp\left(5.0\frac{T_{bp}-T}{T}\right)} \quad (31)$$

Where $P_{bp}$ is the vapor pressure at boiling point, which can be assumed to be at atmospheric pressure unless otherwise noted in the crude oil assay.

Changes to viscosity are handled via an empirical correlation from Mackay et al. (1982) using a reference measurement of oil viscosity.

$$\mu = \mu_{ref} \exp\left[5000\left(\frac{1}{T} - \frac{1}{T_{ref}}\right)\right] \quad (32)$$

Where $\mu$ is the dynamic viscosity and the subscript “ref” describes the reference measurements provided.

# GAS/HYDRATES MODEL

Much like the crude oil, gases are handled in a separate entity to better handle changes to physical properties in a less generalized way. Gases are supplied as molar fractions of the total flowrate by the user from a list of supported gas types which include methane, ethane, propane, butane, hydrogen sulfide, carbon dioxide, oxygen, and nitrogen. Gases are assumed to be well-mixed and in bubbles when gaseous, however the solid forms of methane and ethane are handled separately when hydrate formation begins to occur. Thus, like the crude, properties of the mixed gases are aggregated while hydrate formation and decomposition can add or remove methane and ethane from the mixed gases, changing the overall properties.

## Equations of State

Densities for the gas portion of the plume are calculated using the non-ideal gas law and estimating the compressibility factor using the Brill-Beggs equation with sour gas corrections as described in Guo and Ghalambor (2005) for gas mixtures. In the current implementation of the model the following gases are supported: methane, ethane, propane, butane, hydrogen sulfide, carbon dioxide, oxygen, and nitrogen. The user simply supplies the total volumetric flowrate of the gas mixture and molar fractions of each gas type.

To get density by temperature and pressure using the method outlined in Guo and Ghalambor (2005), first the pseudocritical components must be discerned, which are the critical temperatures and pressures of each gas present averaged by molar fraction. If sour gasses, such

as hydrogen sulfide or carbon dioxide (technically carbon dioxide is an acid gas but for this case treated the same) are present, the following corrections are made.

$$\mathrm{A} = \mathrm{y}_{H_2S} + \mathrm{y}_{CO_2} \qquad B = \mathrm{y}_{H_2S} \tag{33a}$$

$$\varepsilon_3 = 120(A^{0.9} - A^{1.6}) + 15(B^{0.5} - B^{4.0}) \tag{33b}$$

$$T'_{PC} = T_{PC} - \frac{9}{5}\varepsilon_3 \tag{34}$$

$$P'_{pc} = P_{pc} - 6{,}894.7573\left[\frac{P_{pc}T'_{pc}}{T_{PC} - B(1-B)\varepsilon_3}\right] \tag{35}$$

Where $y$ is the molar fraction of a particular gas type; $T'_{PC}$ is the corrected pseudocritical temperature in Rankine; and $P'_{PC}$ is the corrected pseudocritical pressure in PSI. Then, the pseudo-reduced temperature and pressures (the current value divided by the pseudocritical value – denoted by the subscript $pr$), can be used to find the compressibility factor ($Z$) using the Brill-Beggs (1973) equations.

$$Z = A + \frac{1 - A}{\exp(\mathrm{B})} + C \cdot P_{pr}^{D} \tag{36}$$

$$A = 1.39\sqrt{T_{pr} - 0.92} - 0.36T_{PR} - 0.1 \tag{37a}$$

$$B = P_{pr}\left(0.62 - 0.23T_{pr}\right) + P_{pr}^2\left(\frac{0.066}{T_{pr} - 0.86} - 0.037\right) + \frac{0.32P_{pr}^6}{10^E} \tag{37b}$$

$$C = 0.132 - 0.32 \log_{10} T_{pr} \tag{37c}$$

$$D = 10^{F} \tag{37d}$$

$$E = 9(T_{pr} - 1) \tag{37e}$$

$$F = 0.3106 - 0.49T_{pr} + 0.1824T_{pr}^{2} \tag{37f}$$

The compressibility factor gathered from the Brill-Beggs method can be put into the non-ideal gas law to determine the volume from the mass and then calculate density for the mixed-gas bubble.

When properties of individual gases must be known, the Peng-Robinson equations of states are used to determine the compressibility factor and fugacity $(f)$. While the Brill-Beggs is generally sufficient for calculated properties of the gaseous mixture, the Peng-Robinson equations come in handy for hydrate dynamics and dissolution, which must be handled separately for each gas component.

$$Z^3 + (B-1)Z^2 + (A - 2B - 3B^2)Z + (B^3 + B^2 - AB) = 0 \tag{38}$$

$$\ln\frac{f}{P} = (Z-1) - \ln(Z-B) - \frac{A}{2\sqrt{2}B} \cdot \ln\frac{Z + \left(\sqrt{2}+1\right)B}{Z + \left(\sqrt{2}-1\right)B} \tag{39}$$

$$A = \frac{a(T)P}{R^2T^2} \tag{40a}$$

$$B = \frac{bP}{RT} \tag{40b}$$

$$a(T) = \left[1 + \kappa\left(1 - \sqrt{T_r}\right)\right]^2 a_c \tag{40c}$$

$$\kappa = \begin{pmatrix} 0.37464 + 1.54226\omega - 0.26992\omega^2 & \omega \leq 0.49 \\ 0.379642 + 1.48503\omega - 0.164423\omega^2 + 0.016666\omega^3 & \omega > 0.49 \end{pmatrix} \tag{40d}$$

$$a_c = 0.45724 \frac{R^2 T_C^2}{P_C} \tag{40e}$$

$$b = 0.07788 \frac{R T_C}{P_C} \tag{40f}$$

Where $\omega$ is the acentric factor; $T_r$ is the reduced temperature; and the subscript "C" refers to the critical properties. Equation 38 is solved for the compressibility factor $Z$ as a third-order polynomial with at least one real and non-negative root between 0 and 1.

**Gas Bubbles and Slip-Velocity**

Gas bubble size is calculated each timestep and estimated using the non-ideal gas law as given below where $r_b$ is the radius of the gas bubble.

$$P \frac{4}{3} \pi r_b^3 = nZRT \tag{41}$$

To calculate the slip velocity ($w_b$) a harmonic mean approach of two different slip velocity calculations are used as described in Johansen (2000). The slip velocity is calculated as the terminal velocity for rigid spheres in the equations given below.

$$\mathrm{w}_b = \sqrt{\frac{4dg'}{3C_D}} \tag{42a}$$

$$g' = g\frac{\rho_a - \rho_g}{\rho_a} \tag{42b}$$

Where $d$ is the bubble diameter and the ambient density ($\rho_a$) in this case, would be the volume-averaged density of the crude oil and entrained seawater in the control-volume. The drag coefficient ($C_D$) is a function of the Reynolds number and can be calculated in a number of ways. Using the methods described in Johansen (2000), when the Reynolds number is greater than 1000, the drag coefficient is assumed to be 0.44. Otherwise, the drag coefficient is calculated as $C_D = 24/Re$. These two possible drag coefficients are both used in the above equations to calculate the two extreme slip velocities, $\mathrm{w}_1$ and $\mathrm{w}_2$, which are then combined in the equation below with a prescribed maximum set at 0.3 m/s.

$$\mathrm{w}_b = \frac{1}{(w_1^{-1} + w_2^{-1})} \tag{43}$$

The slip-velocity, while it can be ignored in weak cross-flow conditions under the assumption that gas leaving the control-volume is simply replaced from the control-volume below, plays a large role in the separation of gas bubbles in strong cross flows as described in the Jet/Plume Model chapter.

## Hydrates

At great depths, high pressures and low temperatures may allow for the formation of gas hydrates, ice-like structures of water and gas, particularly those formed from methane and ethane, which as a clathrate formation are assumed to form a thin shell around the gaseous bubble. Due to the heat and mass transfers associated with hydrate formation and decomposition, the dynamics of hydrates may have significant effects on the behavior of the jet/plume (Yapa et al. 2001). BLOSOM uses the hydrate kinetics model of Englezos et al. (1987a; b) with the approach described in Yapa et al. (2001) to incorporate the resulting heat and mass transfers.

In BLOSOM, hydrates are calculated for methane and ethane only and hydrates are assumed to be evenly formed and decomposed. Hydrate formation is simulated using the model proposed by Englezos et al. (1987a).

$$\frac{dn}{dt} = KA(f - f_{eq}) \tag{44}$$

Where $\frac{dn}{dt}$ is the formation rate in mols per second; $K$ is the closest formation rate constant provided by Englezos et al. (1987a) for methane and ethane at temperatures from 274-282K; $A$ is the spherical surface-area of the bubble; and $f$ is the fugacity for the dissolved gas in its present state and at equilibrium (subscript “eq”). The difference in this fugacity drives the entire system, thus in the case of the dissolved gas fugacity being less than the equilibrium fugacity, the same equation can be applied for hydrate decomposition, with only the coefficient $K$ changed to a decomposition coefficient, the formulations of which are given in Kim et al. (1987).

## Dissolution

Gas dissolution is calculated using the method described in Zheng and Yapa (2002) for which the dissolution rate is given below.

$$\frac{dn}{dt} = KA(C_s - C) \tag{45}$$

Where $\frac{dn}{dt}$ is the rate of dissolution in mols per second; $K$ is the mass transfer coefficient; $A$ is the surface area of the bubble; $C$ is the concentration of dissolved gas in mols per cubic meter; and $C_s$ is the concentration at saturation or solubility.

The mass transfer coefficient is calculated different for each bubble size-regime (as described in the Terminal Buoyant Velocity subchapter of the Jet/Plume Model chapter. For bubbles in the spherical regime:

$$K = 0.0113\sqrt{\frac{v_t D}{0.45 + 0.2\delta}} \tag{46}$$

Where $v_t$ is the terminal buoyant velocity in cm/s; $D$ is the molecular diffusivity in cm$^2$/s; and $\delta$ is the bubble diameter in cm.

For bubbles in the ellipsoidal regime:

$$K = 0.065\sqrt{D} \tag{47}$$

And for bubbles in the spherical-cap regime:

$$K = 0.069\delta^{-0.25}\sqrt{D} \tag{48}$$

To obtain the solubility, the modified Henry's law from King (1969) as described in Zheng and Yapa (2002) is solved with a known fugacity (from the Peng-Robinson equation of state).

$$f = Hx^l \cdot \exp\left(\frac{10^6 P v^l}{RT}\right) \tag{49a}$$

$$C_s = x^l \rho_a M_w \tag{49b}$$

Where $H$ is Henry's law constant in MPa; $x^l$ is the mole fraction of dissolved gas at equilibrium; $v^l$ is the partial molar volume of gas in solution; $\rho_a$ is the ambient water density; and $M_w$ is the molecular weight of water.

As many of the variables are specific to each gas type, most of the correlations for Henry's law constant, molecular diffusivity, mole fraction dissolved at equilibrium, and partial molar volume must be tracked down for each gas type individually. Some of these values and correlations can be found in Sloan (1997) and King (1969) but are not expanded upon here.

## CONVERSION MODEL

To account for the widths control-volumes can reach once arriving at a terminal level and the generalizations made in a control-volume analysis, proper conversion methods are necessary to break up the control-volume into separate particles with different properties. Failure to consider complexities of this transition could be overlooking a major cause of plumes that peel off and do not surface as the control-volume includes a varied mixture of droplet-sizes and possibly even unmixed crudes.

The conversion model, dubbed the "exploder" model, serves as the intermediary between the control-volume-based Jet/Plume Model and the particle-based Transport Model to help tie together the Jet/Plume and Transport Model while considering the best method of meshing the distinctive modeling approaches. The model oversees the conversion of a 3-dimensional volume into points in 3-dimensional space, taking care to account for the spatial distribution of hydrocarbon density and droplet sizes in the control-volume. As the crude oil is assumed to be well mixed barring input data specifying otherwise, the conversion model distributes volume fractions and associated droplet sizes using the Rosin-Rammler distribution specified in the Jet/Plume Model chapter. The distribution is based off the control-volume geometry and a distribution surface created on top of the control-volume.

A 2-dimensional Gaussian distribution is by default the surface formula for the spatial distribution of oil concentration in the control-volume. The basic equations for such a distribution are given below.

$$PDF(x_{PDF}, y_{PDF}) = \frac{e^{-z/2}}{2\pi\sigma^2} \tag{50a}$$

$$z = \frac{x_{PDF}^2 + y_{PDF}^2}{\sigma} \tag{50b}$$

$$x_{PDF} = {}^{x}/_{r} \qquad y_{PDF} = {}^{y}/_{r} \tag{51}$$

Where $x$ and $y$ are the offset of the desired point from the centroid of the control-volume; $r$ is the radius of the control-volume; and $\sigma$ is the standard deviation which is fixed at $0.\overline{33}$.

Evenly spaced concentric rings of constant value are found using a user-specified minimum width but capped to a minimum and maximum number. Each ring is given a weight based on the PDF value multiplied by the area of the annulus, normalized by the sum of all the rings' PDF values and areas.

$$\mathrm{w}_n = \frac{\mathrm{PDF}_n \cdot \mathrm{A}_n}{\sum(PDF \cdot A)} \tag{52}$$

Where $w_n$ signifies the weight of ring $n$. Each ring becomes a particle sharing the ring's radius and centered in the control-volume, and masses from the entire control-volume are distributed according to the ring weights given. The resulting volume fractions are then plugged in to the reserved Rosin-Rammler distribution for droplet-sizes, using cumulative volume-fraction to get droplet-sizes for each particle.

$$\delta = \delta_{max}\left[\frac{\ln(1 - V_f)}{-2.996}\right]^{1/\mathrm{N}} \tag{53}$$

However, it should be noted there exists an error from the natural log function as the volume fraction approaches 1.0 and the natural log reaches its limit at $\lim_{x\to 0} \ln(x) = -\infty$. Thus, at a volume fraction greater than 0.95, the maximum droplet size is assumed.

The minimum and maximum number of particles created from a control-volume are selected by the user but are by defaults at 3 and 5 respectively. A higher number of particles will mean greater detail in capturing more droplet sizes but also stress the model further as the computational requirements increase.

Initial tests with the conversion model in place showed strong results in capturing variance of plume behavior with each class of droplet sizes peeling off at different levels due to the difference in terminal buoyant velocity. Smaller droplets will have a lower terminal velocity, causing them to rise more slowly or be easily trapped or sunk if there exists a downwards current.

## TRANSPORT & WEATHERING MODEL

Once the plume has reached a terminal level and been properly converted into particles, the spill is transferred into a transport and fate model that simulates the long-term trajectory and degradation of the oil. Transport is driven by advection from winds, waves, and currents, with effects from buoyancy if not surfaced or if sinking. Additionally, particles will undergo turbulent diffusion and stochastic, diffusive movement akin to Brownian motion.

Weathering processes are the physical and chemical changes to the crude include spreading, dispersion, evaporation, emulsification, dissolution, sedimentation, biodegradation, and photolysis, which are depicted in Figure 5. Some processes may only take place on the surfaced oil slicks, while other processes are always present. In light of this BLOSOM maintains records on which particles are surfaced, applying a different set of algorithms for a surface oil slick or submerged droplet cloud.

Lagrangian discrete particles are used to simulate both the oil slick and droplet cloud, with oil slicks seen as a circular area with some thickness on the water surface and droplet clouds as a spherical volume in which oil droplets are present in some concentration. As timesteps can be set independently from the plume model and in the transport model are often much longer (on the order of several minutes or longer), algorithms set in place adjust the first timestep of newly transferred particles to take the appropriate timestep lengths to gradually match up and synchronize to the proper interval.

## Advection & Diffusion

The main means of transporting oil in the far-field is the forcing from currents, and if surfaced, winds and waves. Combined with hydrodynamic models, many of which include surface winds or wind stress, ambient conditions for currents and if necessary, winds, are determined for each particle at every timestep to determine its new drift velocity as given by Shen et al. (1987).

$$\vec{v} = \vec{v}_a + \vec{v}' \tag{54}$$

Where $\vec{v}$ is the drift velocity of the oil parcel, $\vec{v}_a$ is the drift due to advection, and $\vec{v}'$ represents turbulent diffusion. For advection, the drift velocity is computed as below as given in Wang et al. (2005).

$$\vec{v}_a = \alpha_w D\vec{v}_w + \alpha_c\vec{v}_c \tag{55}$$

Where the subset $w$ represents wind and the subset $c$ represents currents; $\alpha$ is an advection coefficient set at 0.003 for wind and 1.0 for currents; and $D$ is a transformation matrix from Wang et al. (2005) that introduces a deviation angle.

$$\mathrm{D} = \begin{pmatrix} \cos\theta & \sin\theta \\ -\sin\theta & \cos\theta \end{pmatrix} \tag{56a}$$

$$\theta = 40° - 8\sqrt{\vec{v}_w}\,, \qquad if\ 0 \le \vec{v}_w \le 25\ m\ s^{-1}$$
$$\theta = 0\,, \qquad if\ \vec{v}_w > 25\ m\ s^{-1} \tag{56b}$$

Horizontal diffusion is simulated using a Monte-Carlo, or random-walk, procedure based on Fisher et al. (1979) wherein a random diffusion velocity ($\vec{v}'$) and angle is added to every particle.

$$\vec{\mathrm{v}}' = R_n\sqrt{4\mathrm{K}_H/t} \tag{57}$$

Where $R_n$ is a randomly generated number from 0-1; $t$ is the timestep in seconds; and $\mathrm{K}_H$ is the turbulent diffusivity coefficient, which can be calculated in a number of ways, but in this case in handled within the Hydrodynamic Handler which calculates horizontal diffusivity based on the Smagorinsky formula (Smagorinsky 1963). This velocity is applied to a randomly generated direction 90° to either side of the parcel's current velocity azimuth.

**Surfacing and Spreading**

On the surfacing of a droplet-cloud, a modified version of equations from Fanneløp and Sjøen (1980) are used for estimating the thickness of the slick that will form.

$$h = \frac{\mathrm{V}}{4.86\pi r v_z} \tag{58}$$

This is double checked against the equation of minimum slick thickness given by Fay (1971) and the slick radius is recalculated from the volume and thickness.

$$h_{min} = 10^{-5}V^{1/4} \tag{59}$$

Spreading is the process of spilled oil on the surface expanding horizontally and thinning out. Most models for spreading are based off the original equations by Fay (1971) where spreading is handled in three, distinct phases: the gravity-inertia phase, the gravity-viscosity phase; and the surface-tension-viscosity phase. However, Fay's equations fail to take into account asymmetrical spreading, the breaking up of a single oil slick into patches, and uneven thickness (Reed et al.

1999). Several modifications and improvements have been developed including a thick-thin slick approach (MacKay et al. 1980), using an elongated elliptical approach (Lehr et al. 1984), and spreading through shear and dispersion processes (Elliot et al. 1986; Johansen 1984).

As in a blowout event most of the spreading occurs underwater, spreading is assumed to be not as significant a process for the transport model. Spreading processes are instead captured through an increased number of particles to capture a multitude of portions of the overall slick that can behave different. Turbulent diffusion, which models the spreading of highly clustered slick parcels such as those given as outputs from the Jet/Plume Model, and dispersion, which has been hypothesized as the reason for the elongated tail to many oil slicks (Delvigne and Sweeney 1988), simulate spreading in a more particle-based scale.

With any degradation process and reduction of the crude, such as with evaporation, the radius is kept constants and the thickness adjusted to fit the changed volume until reaching a minimum thickness as given in Equation 59, at which point the radius decreases instead. In the case of an increase in volume from emulsification, the radius is still held constant under the assumption that the increase in viscosity from emulsification will limit spreading despite an increase in mass.

**Evaporation**

Evaporation can be responsible for as much of 75% or more of the degraded oil mass in just a few days and is the most significant degradation process in the near-term (American Society of Civil Engineers 1996). Originally, analytic and empirical models that required only generalized crude properties were preferred, but with the advent of increased computational power,

pseudo-component evaporation models have come into favor (Reed et al. 1999). Pseudo-component models split the oil into separate fractions of averaged boiling points and compute the evaporation rates of each pseudo-component separately.

Combined with the crude oil model previously described, BLOSOM employs equations by Reinhart and Rose (1982) to determine the mass evaporation rate.

$$\frac{dQ}{dt} = \frac{\alpha Q M_{mol} P_V}{\rho h R T} \tag{60}$$

Where $Q$ is mass of the crude fraction remaining per unit surface area of the slick; $\alpha$ is the mass transfer coefficient; $M_{mol}$ is the average molar mass of the pseudo-component in grams per mol or kg per kmol; $P_V$ is the vapor pressure of the pseudo-component; $\rho$ is the density of the entire mixture; $h$ is the thickness of the slick; and $T$ is the temperature of the slick. It is important to note that $R$, or the gas constant, is for this equation in units of Joules kmol$^{-1}$ K$^{-1}$, which gives a value of about 8,314.46.

The mass transfer coefficient is based on an estimate of sea surface roughness due the wind speeds by Amorocho and Devries (1980).

$$\alpha = C_d v_w \tag{61a}$$

$$C_d = \left(\frac{v_w^*}{v_w}\right)^2 \tag{61b}$$

$$v_w^* = \begin{pmatrix} 0.0323 v_w & if\ v_w < 7\ m/s \\ 0.0323 v_w + 0.7219 \dfrac{v_w - 7}{13} & if\ 7\ m/s \le v_w \le 20\ m/s \\ 0.0474 v_w & if\ v_w > 20\ m/s \end{pmatrix} \tag{61c}$$

Where $v_w$ is the wind velocity and $C_d$ is the drag coefficient. As with no wind velocity no evaporation occurs, a minimum wind velocity of 0.5 m/s is assumed (roughly 1 knot), to coincide with the highest values of the lowest wind class (i.e. calm) on the Beaufort scale, which results in an enforced minimum mass transfer coefficient of roughly $5.216 \times 10^{-4}$. As this is also the assumption if the hydrodynamic data does not include surface winds, evaporation may be underestimated in such a situation.

Alternatively, a technique described by Jones (1997) may be utilized to calculate the volumetric evaporation rate for each distillate fraction, empirically correlated to the molar volume and vapor pressure.

$$\frac{dV_{evap}}{dt} = \frac{v_w^{7/9} V P_V V_{rm} f_m}{h} \tag{62}$$

Where $V_{evap}$ is the volume of the pseudo-component evaporated; $V_{rm}$ is the relative molar volume of the pseudo-component; and $f_m$ is the molar fraction of the pseudo-component. The volumetric evaporation is converted to mass evaporation using the molar mass and molar volumes of the distillate cuts. Likewise, wind speed kept at a 0.5 m/s enforced minimum.

Once mass evaporation is calculated for all pseudo-components, density is recalculated as the volumetric average of the densities of the remaining crude fractions.

## Emulsification

Emulsification, as opposed to evaporation, increases the volume of the slick by process of foaming oil and water into a emulsion through the turbulent action of waves (Reed et al. 1999). The process of emulsification both inhibits evaporation and can increase viscosity by two to three-fold (Lehr 2001). Emulsification can be difficult to quantify as the rates of emulsification and maximum water content can vary by not just the physical properties of the crude, but the specific composition of the crude itself, such as fractional content of waxes, resins, and asphaltenes in the crude.

Using recent research by Fingas and Fieldhouse (2003, 2004), the presence of resins and asphaltenes are used to determine the emulsion's stability class and associated maximum water content.

$$density\ parameter\ (D) = \begin{pmatrix} 0.97 - \frac{\rho}{1000} & if\ \frac{\rho}{1000} < 0.97 \\ 0.97 & if\ \frac{\rho}{1000} = 0.97 \\ \frac{\rho}{1000} - 0.97 & if\ \frac{\rho}{1000} > 0.97 \end{pmatrix} \quad (63a)$$

$$viscosity\ parameter\ (V) = \begin{pmatrix} 8.7 - \ln\mu & if\ \ln\mu < 8.7 \\ 8.7 & if\ \ln\mu = 8.7 \\ \ln\mu - 8.7 & if\ \ln\mu > 8.7 \end{pmatrix} \quad (63b)$$

$$resin\ parameter\ (R) = \begin{pmatrix} 20 & if\ \%_{resin} = 0 \\ 5.4 - \%_{resin} & if\ \%_{resin} < 5.4 \\ \%_{resin} - 5.4 & if\ \%_{resin} > 5.4 \end{pmatrix} \quad (63c)$$

$$asphaltene\ parameter\ (A) = \begin{pmatrix} 30 & if\ \%_{asphaltene} = 0 \\ 12 - \%_{asphaltene} & if\ \%_{asphaltene} < 12 \\ \%_{asphaltene} - 12 & if\ \%_{asphaltene} > 12 \end{pmatrix} \quad (63d)$$

$$class\ number = 0.738 - 0.197D - 0.0126V - 0.0007R - 0.00358A \quad (63e)$$

The resultant class number is then used to determine whether the emulsification if unstable (<0.615), mesostable (<0.66), stable (>0.66), or entrained (>0.64). The entrained and stable state overlap, but the emulsion is considered entrained if the density of the crude oil is greater than 960 kg $m^{-3}$ and the viscosity of the crude oil is greater than 10,000 mPa·s. This information as well as the associated maximum water content for each class is given in

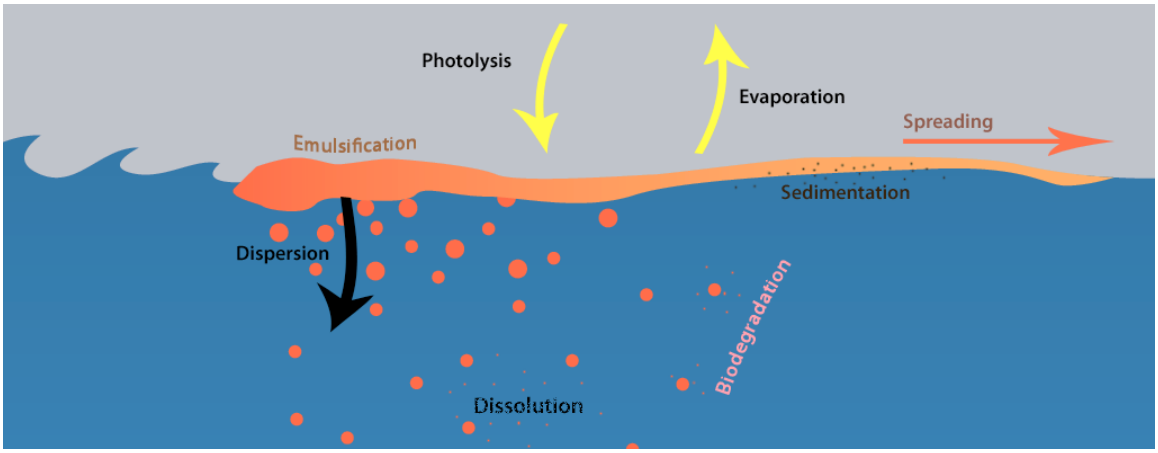


**Figure 5:** Overview of major weathering processes

Table 1.

The first order rate law from MacKay et al. (1980) is employed to determine the entrainment rate based off the maximum water content $(Y_{max})$.

$$\frac{dY}{dt} = 0.0015 A v_w^2 \frac{Y}{Y_{max}} \quad (64)$$

Where $Y$ is the fractional water content; $A$ is the slick surface area; and $v_w$ is the wind velocity. This means the oil begins to emulsify at an increasingly rapid rate until reaching the maximum water content. As the equation does not do anything with a starting value of 0 for the fractional water content, a minimum of 0.01 is assumed. After adding in the new emulsification rate, the fractional water content is checked to ensure it does not exceed the maximum.

Alternatively, the equations from Rasmussen (1985) may be applied which allows for some emulsification even in the presence of no wind.

$$Y = Y_{max}[\, 1 - \exp(-4.5x10^{-6}\, Y_{max}^{-1}\, [1 + v_w]^2\, t_{hr})\, ] \quad (65)$$

Where $t_{hr}$ is the elapsed time in hours, for the model only considering the time in which the parcel was surfaced.

## Dispersion and Sinking

Dispersion is the breaking up of the surface slick through wave action, forcing droplets to entrain back into the water. These droplets may rise immediately causing little change; they may rise slowly, by which time the surface slick has moved horizontally, creating the tail-like spreading effect seen in many oil slicks; or they may not rise at all, instead being too small for their buoyant velocity to overcome turbulent, vertical currents (American Society of Civil Engineers 1996).

The model for the volume of oil dispersed into the water column is based on the equations by Delvigne and Sweeney (1988).

$$Q_{di} = AC^{*}D^{0.57}F_{bw}\delta_{di}\Delta\delta \quad (66a)$$

$$C^{*} = 4450\nu^{-0.4} \quad (66b)$$

Where $Q_{di}$ is the volume entrainment rate for particles of mean diameter $\delta_{di}$; $A$ is the surface area of the slick; $C^{*}$ is a an empirically derived entrainment coefficient tied to the emulsion's kinematic viscosity $(\nu)$; $F_{bw}$ is the fraction of sea surface covered by breaking waves per second; $\delta_{di}$ is the mean diameter of particles in the size class; and $\Delta\delta$ is the particle diameter interval for the size classes.

The dissipated wave energy is approximated by the density of the seawater $(\rho_a)$ and root-means-square wave-height $(H_{rms})$.

$$D = 0.0035\rho_a g H_{rms}^2 \quad (67)$$

The fraction of the sea surface covered by breaking waves is estimated from the wind speed $(\mathrm{v}_w)$ and mean wave period $(T_m)$.

$$F_{bw} = 3x10^{-6}v_w^{3.5}/T_m \quad (68)$$

Wave characteristics such as wave height and mean wave period may be provided by the hydrodynamic model. If not, they may be estimated using empirical equations for wave formation, as described in the Hydrodynamic Handler chapter.

Droplets over a limiting droplet size of 370 µm, as suggested in Reed et al. (2004), are ignored as they are assumed to surface immediately and rejoin the slick. Other droplets require the formation of new Lagrangian parcels below the original slick at the depth of 1.5 times the wave height. These parcels may either rise behind the slick, forming a "tail", or they may be permanently entrained as their limited terminal buoyant velocity does not allow them to resurface.

Alternatively, entire particles may sink due to a combination of increased density from emulsification and disproportionate evaporation of the lighter, more volatile components, leaving behind the heavier residuals. These slicks are assumed to break up into large droplets with a diameter assumed equivalent to the slick thickness and sinking at the rate of the terminal buoyant velocity.

**Biodegradation**

Biodegradation, the degradation of crude oil by bacterial processes, is an extremely slow process that only plays a role in long-term spills. As such, they were often not implemented in oil spill models, but as the Macondo Spill proved, they could be quite significant to the oil budget in extreme spill scenarios (Camilli et al. 2010). However, modeling biodegradation is marred by complexities due to different hydrocarbon components, different bacterial consortiums, and the influences of a plethora of environmental factors, including but not limited to temperature, oxygen, nutrients, and pressure (Atlas 1981).

As such, while biodegradation is desired for BLOSOM, a shortage of methods for simulating biodegradations rates prevented an analytical approach for biodegradation. Instead

biodegradation is estimated with crude oil half-life data when available, and otherwise may be estimated though the rates measured by Walker et al. (1976) for different oil components. However these methods are all still independent of temperature or other environmental factors.

**Other Weathering Processes**

As dissolution and photolysis (the breaking up of hydrocarbons by sunlight into smaller particles) are generally insignificant in the mass balance of oil degradation, they are ignored in the current model. Future simulations may include these are dissolved oil can have significant toxicity impacts even in small quantities, and photolysis may break up more inert, larger hydrocarbons into more volatile components.

Sedimentation is the clinging of water-borne sediments onto oil particles, potentially increasing their density and causing them to sink. While some models have been created, all are dependent on sediment loads data and thus are not currently incorporated into BLOSOM.

Beached oil may also be re-entrained into the ocean due to waves and tides. Along with reintroducing oil back into transport, such crude has often undergone heavy sedimentation, increasing their density and propensity to sink. However, like sedimentation, while some models exists for estimating re-entrainment, they simplify the complex near-shore characteristics, sediment types, wave environment, and other local factors (Reed et al. 1999). Thus re-entrainment rates are not currently implemented until more flexible models for limited shoreline data can be found.

**Changes to Oil Properties**

Evaporation and emulsification, as well as other degradation processes tend to increase the density and viscosity of the oil. The changes to the density due to evaporation are handled by the Crude Oil Model, whereby in coordination with the pseudo-components evaporation, the densities of the remaining oil are averaged by their respective remaining volumes. The effects of emulsification, meanwhile, are handled by averaging the crude oil density (after changes due to evaporation) and the water density by fractional water content.

In the case of a simplistic crude where no distillate cuts are provided, the change in density due to both evaporation and emulsification are handled with an equation given by Wang et al. (2005).

$$\rho_{k+1} = (1 - Y_w)[(0.6\rho_k - 0.34)F_v + \rho_k] + Y_w\rho_a \tag{69}$$

Where $\rho_{k+1}$ is the density at timestep $k + 1$; $Y_w$ is the fractional water content; $F_v$ is the fraction evaporated; and $\rho_a$ is the ambient water density.

Changes to the surface-tension are handled by an asymptotic expression as given by Wang et al. (2005).

$$\sigma = \sigma_0 \frac{V_r}{V_r + V_{em}} \tag{70}$$

Where $V_r$ and $V_{em}$ refer to the volume of the untransformed oil and the volume of the oil in the emulsion respectively.

Changes to the kinematic viscosity are handled through an equation from Buchanan (1987) and Bommelé (1985) as cited in Wang et al. (2005).

$$\nu_{k+1} = \nu_0 \cdot 10^{4F_v} e^{2.5Y_w/(1-0.654Y_w)} \quad (71)$$

Where $\nu_0$ is the kinematic viscosity at some temperature for the unweathered crude oil, taken to be the kinematic viscosity of the fresh crude at the same temperature.

## Tables & Figures

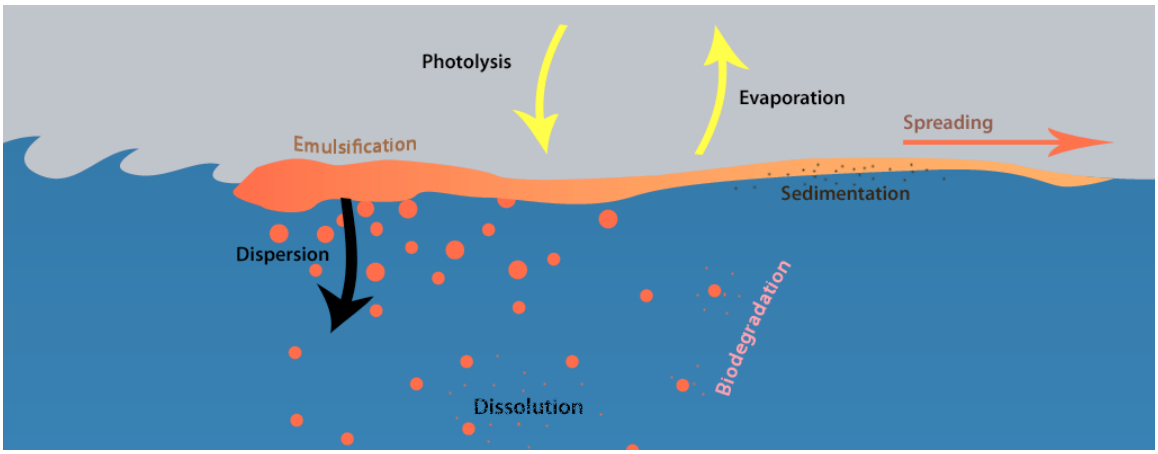


**Figure 5:** Overview of major weathering processes

**Table 1:** Emulsion classes and max. water content (Fingas 2008)

| Class | Class Number | Max. Water Content (%) |
|---|---|---|
| **Unstable** | < 0.615 | 4.1 |
| **Mesostable** | < 0.66 | 17 |
| **Stable** | > 0.66 | 9 |
| **Entrained** | > 0.64 | 17 |

## HYDRODYNAMIC HANDLER

Instead of developing an ocean current model, a handler designed to accommodate outputs from any of the plethora of hydrodynamic models allows BLOSOM to incorporate existing data that may have much more complexity and accuracy (such as real-time updates and corrections from buoys and other observations) or implement an ocean model the user is most familiar with or prefers. In that light, the hydrodynamic handler was designed for flexibility with the various data formats outputted by different hydrodynamic models. In its current state, the hydrodynamic handler can read both geo-referenced rasters such as GeoTIFFs (Geographic Tagged Image File Format), NetCDF (Network Common Data Form) file formats, or a simplistic tabular format of properties by depths (but no variability in the horizontal direction). A consistent naming and folderpath pattern must be employed if data spanning multiple dates are to be used but the pattern itself can be defined by the user and specified in the model settings.

Between depths, the hydrodynamic handler interpolates linearly whereas on a horizontal plane, the handler uses bilinear interpolation to gather values between data points. Temperature and salinity at the bare minimum must be provided by the input data, but estimates of in-situ density, heat capacity, interfacial-tension, and dynamic viscosity can be calculated within the handler using a series of empirical correlations.

A separate bathymetry raster may be provided so as to determine when oil particles are considered beached or settled on the ocean floor, however if not provided, the model can simply uses no-data points in the hydrodynamic data. Should a particle move past the extent of

the hydrodynamic data, the particle is marked as inactive with the simulated time of stoppage stored while the rest of the model continues to simulate.

As seawater density is greatly affected by temperature, salinity, and pressure, in-situ densities for the ambient water are calculated with an empirical correlation using the secant bulk modulus ($K$) (Fofonoff and Millard 1983).

$$\rho_{T,S,P} = \frac{\rho_{T,S}}{1 - P_{bar}/K} \tag{72}$$

$$\begin{aligned}\rho_{pw} = {} & 999.842594 + 6.793952x10^{-2}T_{\circ C} - 9.09529x10^{-3}T_{\circ C}^2 \\ & + 1.001685x10^{-4}T_{\circ C}^3 - 1.120083x10^{-6}T_{\circ C}^4 \\ & + 6.536332x10^{-9}T_{\circ C}^5\end{aligned} \tag{73}$$

$$\begin{aligned}\rho_{T,S} = {} & S\big(0.824493 - 4.0899x10^{-3}T_{\circ C} - 7.6438x10^{-5}T_{\circ C}^2 \\ & - 8.22467x10^{-7}T_{\circ C}^3 + 5.3875x10^{-9}T_{\circ C}^4\big) \\ & + S^{1.5}\big(-5.72466x10^{-3} + 1.0227x10^{-4}T_{\circ C} \\ & - 1.6546x10^{-6}T_{\circ C}^2\big) + 4.8314x10^{-4}S^2 + \rho_{pw}\end{aligned} \tag{74}$$

$$K_{T,S,P} = K_{T,S} + AP_{bar} + BP_{bar}^2 \tag{75}$$

$$A = A_{pw} + S\left(2.2838x10^{-3} - 1.0981x10^{-5}T_{\circ C} - 1.6078x10^{-6}T_{\circ C}^{2}\right) + 1.91075x10^{-4}S^{1.5} \quad (76a)$$

$$A_{pw} = 3.239908 + 1.43713x10^{-3}T_{\circ C} + 1.16092x10^{-4}T_{\circ C}^{2} - 5.77905x10^{-7}T_{\circ C}^{3} \quad (76b)$$

$$B = B_{pw} + S\left(-9.9348x10^{-7} + 2.0816x10^{-8}T_{\circ C} + 9.1697x10^{-10}T_{\circ C}^{2}\right) \quad (77a)$$

$$B_{pw} = 8.50935x10^{-5} - 6.12293x10^{-6}T_{\circ C} + 5.2787x10^{-8}T_{\circ C}^{2} \quad (77b)$$

$$\mathrm{K}_{T,S} = S\left(54.6746 - 0.603459T_{\circ C} + 1.09987x10^{-2}T_{\circ C}^{2} - 6.167x10^{-5}T_{\circ C}^{3}\right) + S^{1.5}\left(7.944x10^{-2} + 1.6483x10^{-2}T_{\circ C} - 5.3009x10^{-4}T_{\circ C}^{2}\right) + 4.8314x10^{-4}S^{2} + \mathrm{K}_{pw} \quad (78)$$

$$\mathrm{K}_{pw} = 19652.21 + 148.4206T_{\circ C} + 2.327105T_{\circ C}^{2} + 1.360477x10^{-2}T_{\circ C}^{3} - 5.155288x10^{-5}T_{\circ C}^{4} \quad (79)$$

Where the subscript “pw” indicated pure-water; $S$ is salinity in PSU; $T_{\circ C}$ indicates a Celsius value for temperature; and $P_{bar}$ indicates bar values for pressure.

Pressure may be calculated using one of three possible methods, each having some unique balance of accuracy and computing speed, the simplest being the oceanographic rule of thumb of an increase of one decibar for every 1.019716 meters depth and the most complex involving

integrating using all available depth values given in the hydrodynamic data. For simulations in this paper, pressure was calculated using the ambient density at the location of the control-volume ($P = \rho_a gh + \rho_{atm}$).

Specific heat ($C_P$), in Joules per kilogram per degree Kelvin, is estimated as a function of temperature and salinity (Fofonoff and Millard 1983). Specific heat increases with temperature and is inversely proportional to salinity and pressure.

$$\begin{aligned} \mathrm{C}_P = {} & 4217.4 - 3.720283T_{\circ C} + 0.1412855T_{\circ C}^2 - 2.654387x10^{-3}T_{\circ C}^3 \\ & + 2.093236x10^{-5}T_{\circ C}^4 \\ & + S\left(-7.643575 + 0.1072763T_{\circ C} + 1.38385x10^{-3}T_{\circ C}^2\right) \\ & + S^{1.5}\left(0.1770383 - 4.07718x10^{-3}T_{\circ C} + 5.148x10^{-5}T_{\circ C}^2\right) \end{aligned} \tag{80}$$

Interfacial tension ($\sigma$), in Newtons per meter, is estimated as a function of temperature and salinity using the correlations provided by Sharqawy et al. (2010).

$$\sigma_{pw} = 0.2358\left(1 - \frac{T_K}{647.096}\right)^{1.256}\left[1 - 0.625\left(1 - \frac{T_K}{647.096}\right)\right] \tag{81}$$

$$\sigma = \sigma_{pw}[1 + (0.000226 \cdot T_{\circ C} + 0.00946) \cdot \ln(1 + 0.0331 \cdot S)] \tag{82}$$

Dynamic viscosity ($\mu$), in Pascals per second, is also estimated as a function of temperature and salinity using the correlations provided by Sharqawy et al. (2010).

$$\mu_{pw} = 4.2844x10^{-5} + [0.157(T_{\circ C} + 64.933)^2 - 91.296]^{-1} \tag{83}$$

$$\mu = \mu_{pw}(1 + A \cdot S + B \cdot S^2) \tag{84a}$$

$$A = 1.474x10^{-3} + 1.5x10^{-5}T_{\circ C} - 3.9275x10^{-8}T_{\circ C}^2 \tag{84b}$$

$$B = 1.073x10^{-5} - 8.5x10^{-8}T_{\circ C} + 2.23x10^{-10}T_{\circ C}^2 \tag{84c}$$

The hydrodynamic handler is also equipped with algorithms to perform some basic vector field calculations, through which it can obtain horizontal diffusivity values based on the Smagorinsky model detailed below (Smagorinsky 1963).

$$\mathrm{K}_H = C_S \Delta x \Delta y \sqrt{\left(\frac{\partial v_x}{\partial x}\right)^2 + \frac{1}{2}\left(\frac{\partial v_x}{\partial x} + \frac{\partial v_y}{\partial y}\right)^2 + \left(\frac{\partial v_y}{\partial y}\right)^2} \tag{85}$$

Where $C_S$ is the Smagorinsky coefficient, by default set to 0.15 and $\Delta x \Delta y$ basically represent the pixel area.

For estimating wave heights and periods, the model uses the following equations from the U.S. Army Corp. of Engineers (Coastal Engineering Research Center 1984).

$$\mathrm{H}_s = 0.0248\tau_w^2 \tag{86}$$

$$\mathrm{T}_p = 0.83\tau_w \tag{87}$$

Where $\mathrm{H}_s$ represents the significant wave-height and $\mathrm{T}_p$ is the peak period of the wave-spectrum. The wind-stress $(\tau_w)$, if not provided, can be estimated with the wind velocity (Coastal Engineering Research Center 1984).

$$\tau_w = 0.71v_w^{1.23} \tag{88}$$

Likewise, the same correlation can be used in reserve if the data provides wind stress but not the explicit wind velocity.

## PLUME MODEL VALIDATION

Both fortunately and unfortunately, there exist few real-life blowout events in which to validate the plume model. Of the two major instances (Macondo and Ixtoc), data on the plume itself is limited or estimates of the blowout conditions highly-contested, making them poor choices for a validation. However, a limited number of field-experiments do exist, on one of which the plume model for BLOSOM was validated against.

On August 1995, the IKU Petroleum Research organization (now SINTEF), conducting an oil plume experiment in the Frigg field in the North Sea, released oil from a submerged pipe for 25-minutes (Rye and Brandvik 1997). Oil was released at 107 meters depth with temperature and salinity measured every 10 meters starting at 100 meters depth and currents measured roughly every 30 meters starting at 80 meters of depth at the deepest. Plume width and elapsed time were analyzed at depths of 10 meter intervals starting at 100 meters using video and sonar recordings with an end to jet-like behavior observed at between 50-60 meters depth (Rye and Brandvik 1997). Figure 6 overviews the measurements made during the field experiment.

A second field experiment was conducted the following year with gas (air) being injected with the crude. This caused a significant increase in the plume's rate of rise and introduced oil/gas dynamics, although the formation of hydrates was extremely unlikely. However, a lack of seawater and current measurements and unavailability of the ROV plume measurements for this experiment did not provide enough data to run a validation.

## Methods

Rye and Brandvik (1997) and Rye et al. (1996) provided data on the field experiment carried out in the North Sea in 1995 that were used in validating the model. Temperature ranged from 7.5°C at 100 meters depth to 14.7°C at the surface. Salinities ranged from 35.3 to 34.4 PSU. Currents stayed under 0.1 m $s^{-1}$ but varied greatly in direction, often nearly reversing direction at each measurement point. Currents, temperatures, and salinities were linearly interpolated between measurements. Details of release conditions and ocean profiles are given in

Table 2 and Table 3.

This experiment was recreated on the Jet/Plume Model previously described using the provided data from Rye and Brandvik (1997) and Rye et al. (1996). Timesteps were set to 1 second, and all coefficients were set to their default values. A simplified crude oil was supplied, using the API gravity of 26.95 that matched the given crude density. As no weathering occurs in the plume model, the lack of the pseudo-components approach to crude model had no effect.

## Results

Figure 7 displays a comparison between the modeled plume and field observations. The model simulated a terminal-level of 55.17 meters depth with a plume width of 27.7 meters, agreeing with the range of the observed terminal level and the rounded width of 30 meters at 60 meters depth. The simulated time to reach the terminal level was 5 minutes and 38 seconds, compared to the estimated 5 minutes observed in the field to reach the closest measured depth of 60m. A

maximum droplet size of 6.25mm was simulated compared to the estimated maximum observed droplet size of 5mm given in Rye et al. (1996).

For some simulations, the plume model was allowed to continue to run after reaching the terminal level (without transferring to the Transport Model) as it proved a decent test of the jet-coefficient to observe if it could effectively continue to model the plume as a droplet cloud. After 8 minutes, the plume was at about 46.5 meters depth with a width of over 33 meters. The observed conditions reached a depth of 40 meters and a width of roughly 35 meters after 8 minutes.

**Discussion**

It is interesting to note that during the plume model validation, the plume suddenly widens when just above 80 meters depth. In subsequent tests removing the jet-coefficient, this event disappears. Such a behavior matches well with the sudden jump in plume width observed from 80 to 70 meters depth, where the plume rapidly expands about 10 meters horizontally and was not duplicated in simulations with other plume models as seen in a similar validation by Yapa et al. (2001).

Horizontal displacement deviated from the observed data, especially towards the end. This is most likely the result of uncertainties given in the measured currents. As no currents were measured below 80 meters depth, currents with assumed to be constants from 80 meters down, and currents between measurements (spaced 30 meters apart) were linearly interpolated, where often near reversals in direction suggests much more complicated current

patterns than could be ascertained from the data given. Furthermore, the displacement was observed only on a single axis (a northwest to southeast line), and observations from other angles may have provide stronger agreement with the actual experiment. It appears that currents may have been stronger towards the southeast than expected, which if true, would also have contributed to more entrainment and hence the generally smaller widths modeled compared to what was observed.

Overall, the Jet/Plume Model gives strong results that at worst, seem to share the same discrepancies as other validations done on this dataset and at best, capture behaviors not simulated before. This simulation provides a strong case for the accuracy of the newly implemented jet-coefficient and validates the use of shearing rather than bending control-volumes. Further tests with mixed-gas plumes and a deeper depths would be ideal, but at the moment are limited by a lack of spatially-explicit data on the 2$^{nd}$ North Sea field-experiment or the DeepSpill experiment.

## Tables & Figures

**Table 2:** Field release conditions (Rye and Brandvik 1997)

| | |
|---|---|
| Source depth | 107 m |
| Outlet diameter | 0.1016 m |
| Release rate | 1 $m^3 min^{-1}$ |
| Initial velocity (vertical) | 2.1 m $s^{-1}$ |
| Initial oil density | 893 kg $m^{-3}$ |

**Table 3:** Measure ambient conditions for field experiment (Rye et al. 1996)

| Depth (m) | Temp. (°C) | Salinity (PSU) | Density ($kg/m^3$) | Velocity (m/s) | Azimuth (degrees) |
|---|---|---|---|---|---|
| **0** | 14.7 | 34.4 | 1025.6 | 0.01 | 152 |
| **10** | 14.7 | 34.5 | 1025.7 | | |
| **20** | 14.1 | 34.6 | 1025.9 | 0.07 | 87 |
| **30** | 11.0 | 34.9 | 1026.7 | | |
| **40** | 9.8 | 35.2 | 1027.1 | | |
| **50** | 9.1 | 35.3 | 1027.3 | 0.01 | 171 |
| **60** | 8.6 | 35.3 | 1027.4 | | |
| **70** | 8.3 | 35.3 | 1027.5 | | |
| **80** | 7.9 | 35.3 | 1027.6 | 0.03 | 30 |
| **90** | 7.5 | 35.3 | 1027.6 | | |
| **100** | 7.5 | 35.3 | 1027.6 | | |

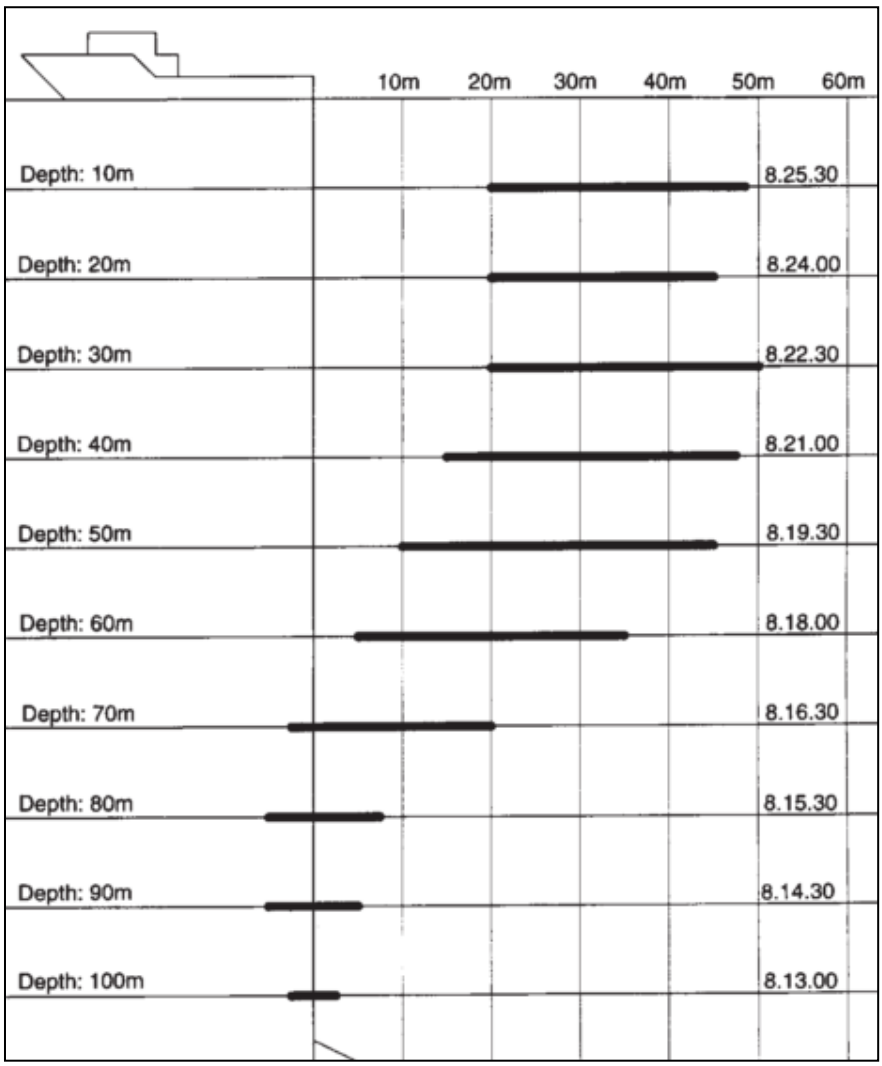


**Figure 6:** North Sea Experiment measurements (adapted from Rye and Brandvik 1997)

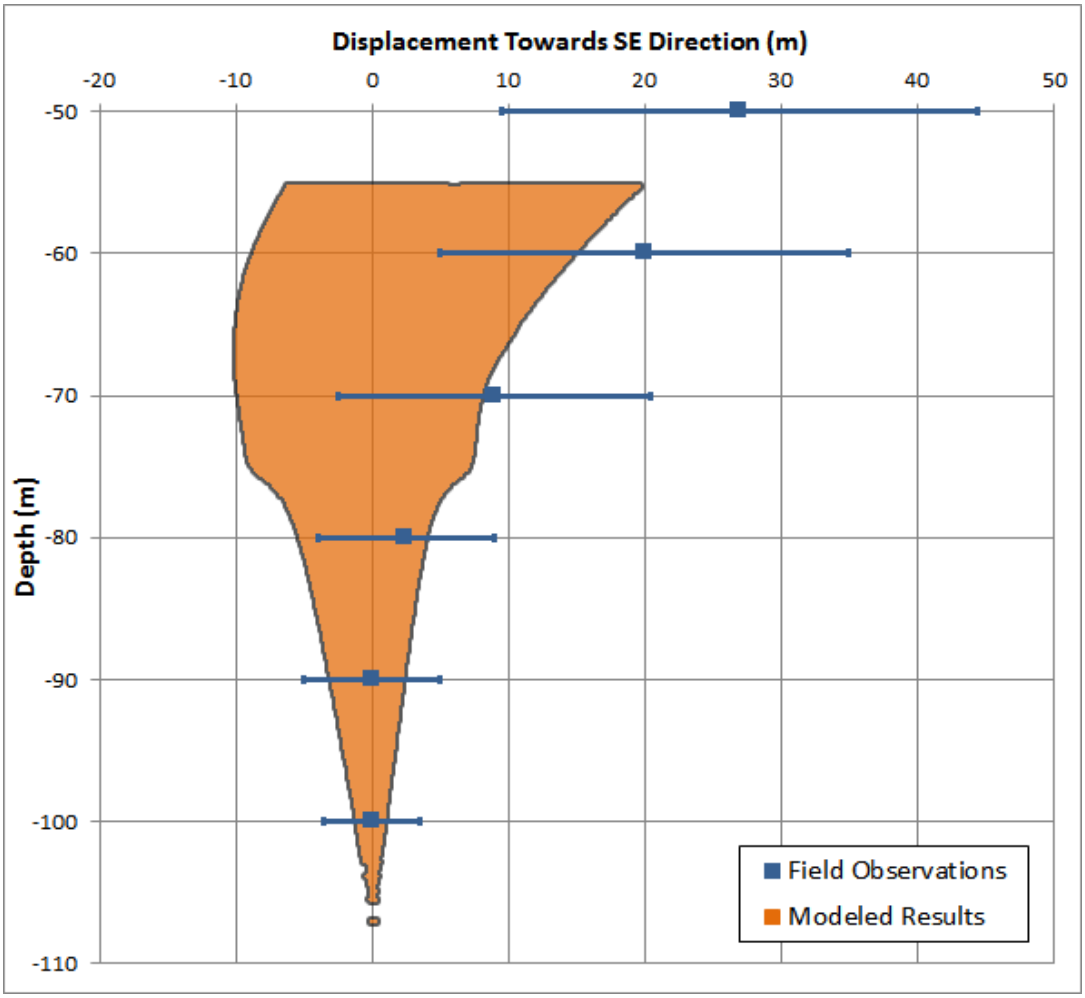


**Figure 7:** Modeled jet/plume compared with field observations given in Rye and Brandvik (1997)

# APPLICATION IN THE GULF OF MEXICO

As the Gulf of Mexico is the major site for deepwater and ultra-deepwater oil exploration in the United States, it was chosen as a prime location for an example model application. The exact site chosen was located in the Mississippi Canyon region, on the edge of the continental shelf, where a significant number of the recent deepwater and ultra-deepwater discoveries have been made, including Macondo Prospect, Aconcagua, and Thunder Horse and totaling 572 ultra-deepwater leases.[2] The combination of high production in the area and proximity to the coast provide a prime location for the testing of a hypothetical blowout location.

The latitude and longitude for the exact site chosen sits at approximately 28.68°N and 89.14°W, on Outer Continental Shelf (OCS) block 281. The site lies 74 km west of Macondo Prospect and is located only about 45 km from shores of the Mississippi Delta. The depth of the prospective well is located at about 1,200ft (366m) beneath sea level, classifying it as a deepwater well.

## Methods

A crude was chosen based on similarity to the type expelled by Macondo, with an API (American Petroleum Institute) gravity estimated to be around 34-39 (Lehr et al. 2010) – which equates to a STP, or standard temperature (15°C) and pressure (1 atm), density of roughly 830-855 kg $m^{-3}$. Alaskan North Slope (ANS) with an API gravity of 32 and a STP density of about 865 kg $m^{-3}$ was

[2] Bureau of Ocean Energy Management (BOEM) (2013). "Leasing Information." <http://data.boem.gov/homepg/data_center/leasing/leasing.asp> (14 August 2013).

used as it was within the same range though slightly heavier. An assay provided by British Petroleum gave measurements for eight usable distillate cuts covering roughly three-quarters of the crude by volume fraction. The residual pseudo-components for the last quarter were determined by interpolations and overall gave ten pseudo-components with densities at STP ranging from 690 to 976 kg $m^{-3}$ and a recalculated STP density for the entire crude at 864 kg $m^{-3}$.

The blowout conditions were arbitrarily set, with a blowout diameter of 0.4 meters and a flowrate of 74.5 kg $s^{-1}$, equivalent to just under 62,500 barrels per day. The release velocity was set at 2.4 m/s upwards and a temperature of 30°C. No gases or water was assumed to be in the current mix. The blowout was set to start on the 20$^{th}$ of April 2010 at 13:45 GMT with a 24-hour duration. Transport Model timesteps were set to 5 minutes and Jet/Plume Model timesteps at 10 seconds.

For the hydrodynamic data, outputs from the Intra-America Seas Nowcast Forecast System (IASNFS), an implementation of the Navy Coastal Ocean Model (NCOM), were utilized, giving a 3.6 km resolution horizontally, twenty-eight depth layers at increasing intervals from 0 to 4,000 meters depth, and a 6-hour temporal resolution. Unfortunately the outputs given did not include surface wind velocities or wind stress, so many of the wind dependent processes were either insignificant or in the case of evaporation, forced to a minimum but likely underestimated. Future runs will likely switch over to the outputs given by the AmSeas implementation of the NCOM, which includes wind stress, an increased spatial-resolution of 3 km, and an increased temporal resolution of 3 hours.

To test the sensitivity introduced by different blowout conditions, two more runs were implemented with two modified parameters that would directly affect the droplet-size distribution, those being a smaller blowout diameter and a mixed-gas blowout respectively. The second run used a blowout diameter of 0.1 meters while the third run utilized a gas flowrate of 50.0 kg $s^{-1}$ distributed by mass between methane (30 kg $s^{-1}$), ethane (10 kg $s^{-1}$), propane (5 kg $s^{-1}$), and butane (5 kg $s^{-1}$) in addition to the decreased blowout diameter. Other than the indicated differences, all other settings were kept the same as the original model run.

**Results**

The initial mass expelled by the blowout after the 24-hour period was 6,436,800 kg. Up to 50% of the spill quickly evaporates in the first five days, and by the end of the 40-day run, a majority of the active particles (not beached or sunk) have undergone over 90% evaporation. Table 4 outlines the oil budget until the end of the first simulation.

The terminal level for the jet was at around 165 meters depth. While the distribution of droplet-sizes meant some plumes rose slower and were caught in subsurface currents for a longer period, all droplets eventually surfaced with an initial rise time of about 30 minutes. The maximum droplet-size was roughly 10 mm with the parameters for the conversion model splitting each control-volume into an average of three parcels with 3 mm as the lowest distributed droplet size, both of which are relatively large sizes in the spherical-cap regime, and contributed to high terminal buoyant velocities. As such, after the first two days, the spill is entirely relegated to the surface with no lingering subsurface plumes.

There was very little emulsification and no dispersion due to the lack of winds or waves data. Some emulsification did occur using the minimum wind values, but all dispersed droplets did not go under the minimum size for which they were not assumed to rejoin the slick immediately.

Spatially, the oil undergoes remains in a relatively homogenous, if very twisted, shape for the first several days before being pulled apart by the complexities of the nearshore currents. Due to the proximity to the shore, many particles beach by the 2$^{nd}$ day after being pushed into the Mississippi Delta. However, the currents shift outwards soon afterwards, sending most of the spill offshore. Other parts of the spill continue northwards, endangering the areas of Gulfport and Mobile Bay along the Mississippi and Alabama coasts. Figure 8 and Figure 9 map the trajectory of the spill and locations of beaching.

Shortly after day 15, the spill encounters and Loop Current and is quickly pulled towards the Southeast. By the end of the 30 days, the spill has entered the Gulf Stream with some beaching in the Florida Keys and by the end of the model run at 40 days, significantly particle beaching has occurred in Florida and many particles have moved out of the extent of the IASNFS dataset. However, many of the particles have undergone over 80% evaporation by this point. With other degradation processes such as biodegradation not factored in the current model, it is possible that not enough oils would actually remain to seriously threaten the environment here.

The second model run, using the smaller blowout diameter, resulted in a maximum droplet-size of roughly 5.7 mm, which created parcels with a distributed droplet size as low as 1.7 mm, which while significantly smaller than the original simulation, are still relatively larger droplets. Thus, while the droplets took longer to surface, by the end of the second day, all parcels had

surfaced and there appeared to be no lingering subsurface plumes. Figure 10 showcases the distribution of the spill for the second model run for the first 20 days, which was near identical to the first model run. The time to reach the surface was roughly 35 minutes and the terminal level for the jet at about 175 meters depth.

The third model run, with mixed gases as well as the narrower blowout diameter, resulted in a maximum droplet-size of just under 3 mm. The smallest distributed droplet-size was just under a millimeter at 0.91 mm. The terminal level for the jet was simulated at 168 meters depth and the blowout took about 40 minutes to surface. Due to crossflow conditions, most of the gases separated and left the plume after traveling 20 meters vertically. Despite the smaller droplet sizes, the spatial distribution ended up very similar (Figure 11) and as with the previous model runs, no long-term subsurface plumes were simulated. Minute differences were apparent due to the randomness of the turbulent diffusion processes, but did not play as major a role in the overall distribution of the spill. The most noticeable differences were in the locations and extents of beaching along in the regions of Gulfport and Mobile Bay, but much of these can likely be attributed to the stochastic nature of the turbulent diffusion process as these are only a handful of particles.

In all cases, the total number of particles created by the model was at 25,707.

## Discussion

The trajectory of the spill, the extent of the spill, and locations of beaching all hinge significantly on the variability of the currents in the region. As the bulk of the spill occurred before the Loop

Current had separated into Eddy Franklin in late May, a large portion of the spill is drawn into the Florida Straits. Had the blowout occurred somewhat later the probability of the spill entering the Gulf Stream becomes quite small as at worst it would likely own be drawn into the eddy that pinches off of the Loop Current and remains mostly stationary. Likewise, a continuous or extended blowout beyond what was simulated would likely have the majority of its spill get trapped within Eddy Franklin, away from major coasts. As such, the time of blowout, location, seasonality, and pattern of the currents play a large role in the variability of the potential spill extents.

Unfortunately, wind advection could not be simulated due to the hydrodynamic outputs for the time period not supplying such data, further model runs on the newer AmSeas data (another implementation of the NCOM model for the Gulf of Mexico region that supplanted IASNFS in 2011) with wind stress data will likely show other patterns and diffusive effects as surfaced oil may be scattered out of the currents.

Evaporation works with great celerity, as expected in a relatively light crude given its high API gravity and low density, but even this may be underestimated due to lack of wind data. On the other hand, when many points are clustered together, the approach used by the model may overestimate evaporation due to ignoring overlap and over-calculating surface area. Both for greater accuracy here and improved performance, an algorithm to combine nearby particles into one will be sought for future implementations of BLOSOM.

Due to the lack of wind data and the use of the minimum wind evaporation may have been at time both underestimated and overestimated. As winds factor directly into the evaporative rate,

the rate of evaporate due to winds was likely underestimate. However, as winds also play a role in emulsification, which inhibits evaporation, use of the minimum wind values underestimated emulsification which in turn may have overestimated evaporation. Thus, the need to switch to the more detailed AmSeas outputs with wind stress data is evident; however those datasets will only have data from late 2010 onwards.

The lightness of the crude likely contributed to a lack of non-surfacing plumes as even its heaviest pseudo-component was significantly lighter than the ambient seawater. Besides a generally larger droplet size distribution due to the initial conditions given – particularly a large blowout diameter and lack of gases – this suggests that to simulate non-surfacing plumes and/or sinking oil, other processes may be playing a role. Sedimentation may be one likely culprit, which may be quite high in a region just off the Mississippi Delta. Emulsification processes may also be at work during the jet phase, something not currently captured in the model, meaning that oil parcels are weighted down by the heavier waters entrained from near the ocean bottom.

Generally speaking however, droplet-sizes in all model runs were quite large resulting in too high of buoyant terminal velocity values for subsurface plume development. While the distribution may be accurate, due to the method of distributing droplet-sizes, only sizeable chunks by volume fraction of the droplet-size distribution could be divvied out to the parcels created from control volumes. As a result, the minimum droplet-size observed in the parcels did not drop far below the 1mm range. For comparison, simulations by North et al. (2011) with user defined droplet-sizes best reproduced the subsurface plumes observed by Camilli et al. (2010) following the Macondo blowout when modeling droplet-sizes in the ranges of 10-50 μm.

The volume fraction of droplets with that small of diameters may not be significant in each individual control-volume, but in a long-term spill the accumulation of such small droplet distributions over time seems important to capture. Modifying the conversion model to instead of breaking up the droplet-size distribution by equally spaced volumetric fractions but by pre-defined size-breaks of which major differences in droplet behavior occur may then by more apt. The next stage then would be to properly identify these breaks in a way that balances the ability to capture the varied behaviors across the droplet-size distribution with the need to optimize the computing speed by not over-creating particles and slowing down the simulation.

Furthermore, the lack of current data in the vertical direction meant that even very small droplets of very low buoyant terminal velocity would still eventually surface, if very slowly. Unfortunately, even the new AmSeas outputs do not provide vertical currents. This may require an algorithm for simulating vertical diffusion or estimates of vertical currents through analysis of divergence and convergence and/or mass flow rates at the same location for consecutive depth layers to estimate the flow in the vertical direction.

The model did not appear to be highly sensitive to the blowout conditions, at least for the parameters tested. While different rise times may have cascading effects as droplets linger longer in subsurface currents and change in trajectory, this did not appear to be the case in the three tested simulations. Some of this may be attributed to the fact that while the blowout location was technically deepwater, the depth was not particularly deep at only about 1,000 ft. The resulting rise times between the three models only differed by about 5 minutes each and as a result the vertical dimension of simulations did not prove as significant a factor in the spill.

Further tests with even deeper blowout locations and varied blowout velocities could likely show higher sensitivities, but overall, the results display a remarkably tight envelope on the uncertainty with the blowout conditions tested. Lack of data or uncertainties on the exact blowout parameters appear not to be as consequential as the seasonality which is beneficial for both immediate response and potential risk modeling applications with large uncertainties.

## Tables & Figures

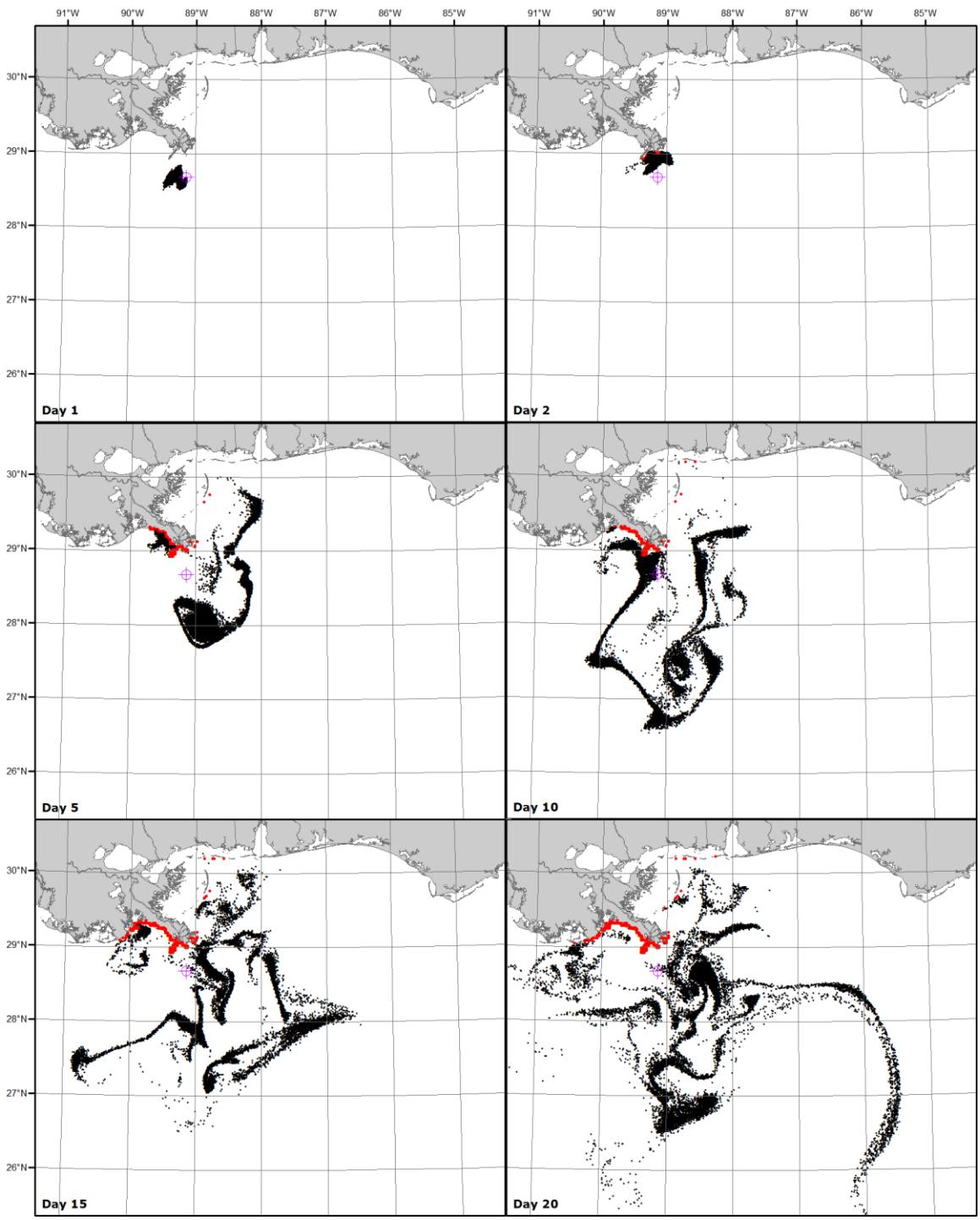


**Figure 8:** First model run day 1 to 20 (cross indicates blowout site)

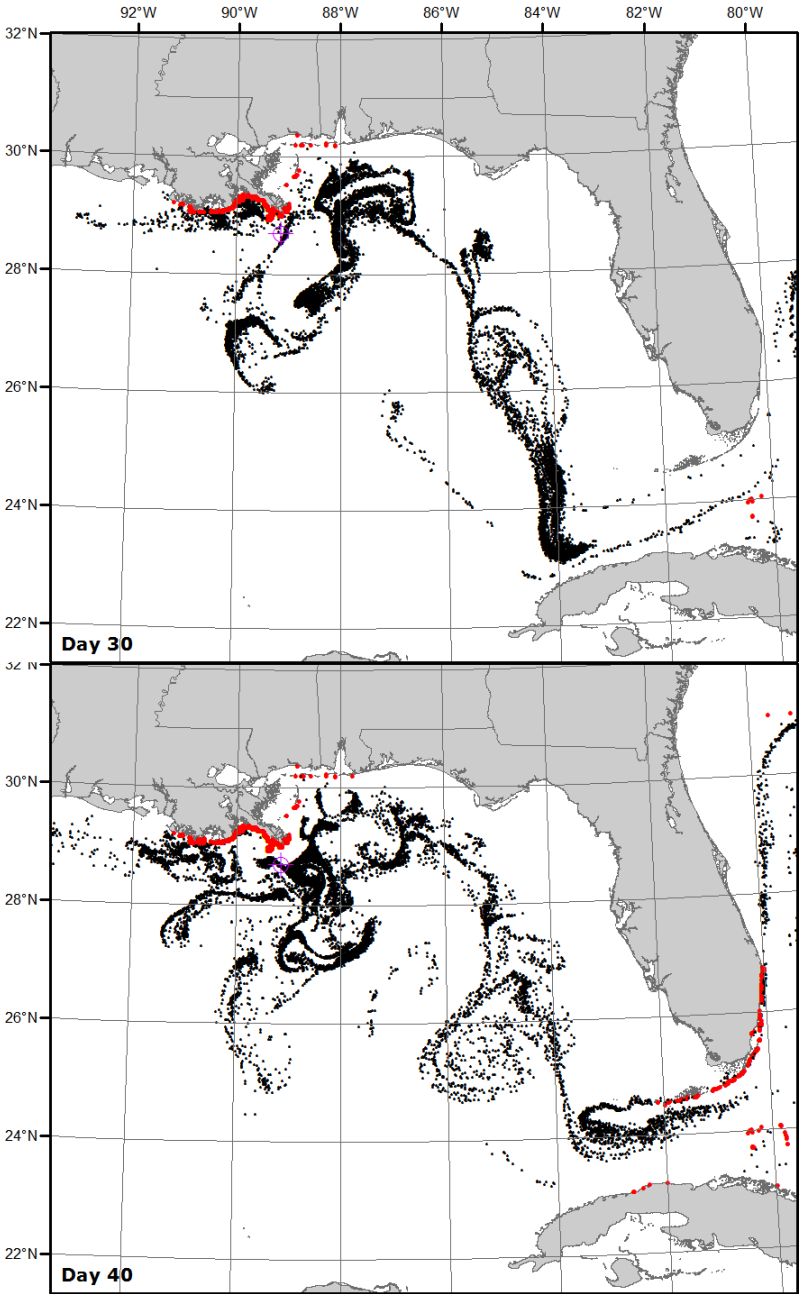


**Figure 9:** First model run day 30 and 40 (note change in scale/extent)

**Table 4:** Oil budget (all numbers in kilograms or unitless fractions)

| Days | Total Mass (active) | Total Mass (beached) | Total Mass (evaporated)* | Fraction Evaporated (of total)* | Fraction Evaporated (of active) | Fraction Beached |
|---|---|---|---|---|---|---|
| **1** | 5,039,806.0 | 0.0 | 1,396,994.0 | 0.22 | 0.22 | 0.00 |
| **2** | 3,955,150.3 | 79,787.9 | 2,401,861.7 | 0.37 | 0.37 | 0.01 |
| **5** | 2,686,674.0 | 494,373.9 | 3,255,752.0 | 0.51 | 0.51 | 0.08 |
| **10** | 1,919,483.2 | 766,592.3 | 3,750,724.5 | 0.58 | 0.61 | 0.12 |
| **15** | 1,532,955.4 | 859,721.9 | 4,044,122.7 | 0.63 | 0.67 | 0.13 |
| **20** | 1,302,120.8 | 876,713.2 | 4,257,966.0 | 0.66 | 0.72 | 0.14 |
| **30** | 1,020,965.1 | 896,298.8 | 4,519,536.1 | 0.70 | 0.78 | 0.14 |
| **40** | 772,101.7 | 957,625.5 | 4,707,072.8 | 0.73 | 0.82 | 0.15 |

*This number does not account for beached crudes that continue to evaporate

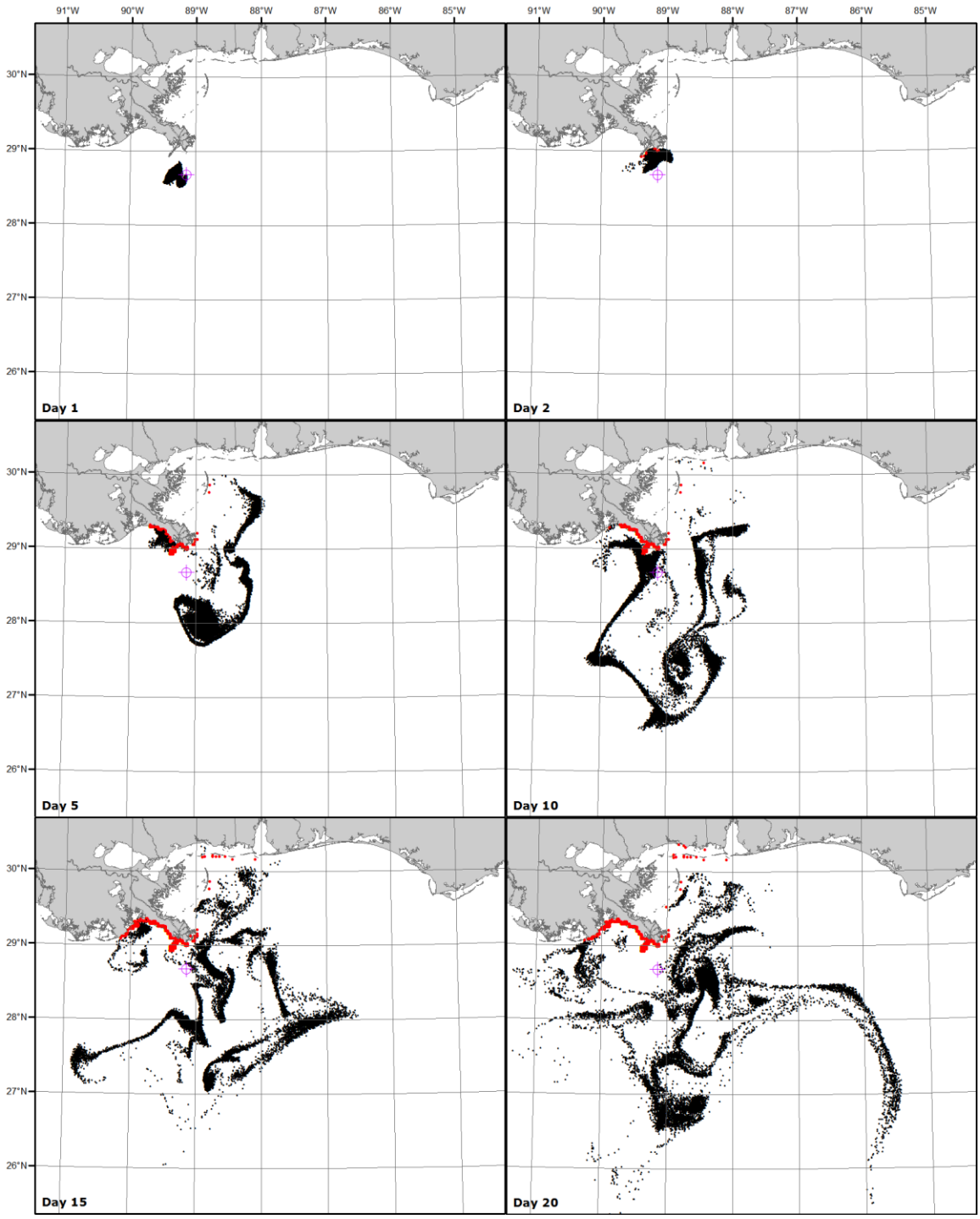


**Figure 10:** Second model run (cross indicates blowout site)

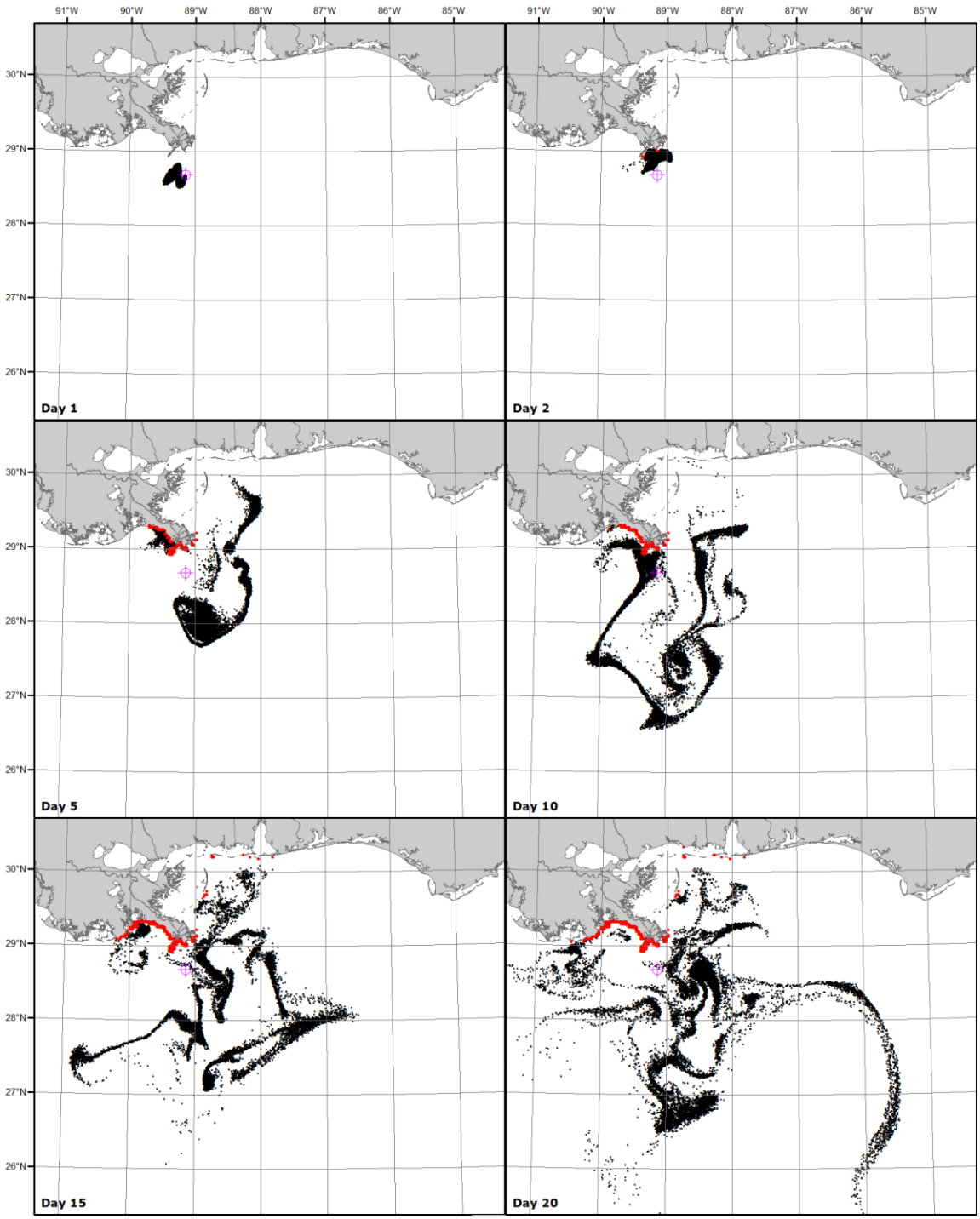


**Figure 11:** Third model run (cross indicated blowout site)

# CONCLUSION

BLOSOM represents an approach to spatially-explicit and comprehensive model for deepwater and ultra-deepwater blowouts, both in response to the Macondo incident and in light of the need for risk-assessment and impacts-oriented models. To achieve this goal, BLOSOM was built from the ground up to incorporate the latest in techniques for simulating multi-phase plumes, gas/hydrates, transport, and weathering as well as to provide a framework for allowing the adaptability and flexibility required for risk assessment and the outputs required for impact/toxicity models down the line. This necessitated a series of relatively independent but well-coordinated model components, that besides the traditional transport and fate components, also handled flexible hydrodynamic inputs, in-depth management of crude mixtures, and new algorithms for handling the transitions between components with contrasting modeling approaches.

The Jet/Plume Model handles the near to intermediate-phases of the blowout where a mixture of buoyant crude oils and gases rise as first a momentum-dominated jet into a more buoyancy-dominated plume. Here high-pressure equations-of-state, modifications to the original Lagrangian control-volume approach, and handling of gas hydrates give BLOSOM added accuracy for deepwater and ultra-deepwater blowouts. The use of the jet-coefficient, a new and more dynamic approach to regulating entrainment, and a unique and purpose-designed conversion model allow for the most robust transition in the intermediate-phase and when transferring elements from the control-volume-based Jet/Plume Model to the parcel-based Transport Model.

Beneath these main components, the Crude Oil Model and Gas/Hydrates Model help to predict changes of the physical and chemical properties of the crude through weathering processes and at different temperatures and pressures using a series of correlations and equations-of-states, each chosen for the best accuracy to the application at hand. The Crude Oil Model in particular allows for the prediction and interpolation of the crude's properties – both aggregated for the mixture and for each distillate cut – based on readily-obtainable crude assay data or even from best estimates of crude composition. This allows for more accurate handling of changes to the crude, particularly during degradation processes that affect different distillate fractions disproportionately, and a better picture in the outputs of the crude components remaining for potential impacts and toxicity modelers.

Both fortunately and unfortunately, the availability of data to validate against for a blowout model proves sparse. Few events even exist, and of those that do, data is limited. The Ixtoc Spill lacks spatially-explicit data accurate enough for a validation of this type. The Deepwater Horizon/Macondo Spill has still conflicting reports on flowrates and composition, lack of data on sub-surface plumes, and as of this writing is still embroiled in complications with legal issues in simulating against due to the ongoing case against British Petroleum. Fortunately, some field-experiments conducted specifically for research and data on blowout dynamics provided some validation data against with BLOSOM could be run. The North Sea experiment, tested against BLOSOM's Jet/Plume Model, showcased the robustness of the model and in particular validated the implementation of the newly-developed jet-coefficient.

A test application run in the Gulf of Mexico provided both the results for a potential blowout spill and some insights into the uncertainty and sensitivity of the model to blowout parameters.

The model, at least for the location simulated, did not appear highly sensitive to blowout diameter or gas content, though these may play progressively larger roles in deeper blowouts. Instead, seasonality of the currents played the biggest role in the distribution of the spill. Some stochasticity was noted in the exact locations of beached crude, but the overall picture of regions endangered remained consistent. These results allow a relatively higher degree of confidence when simulating blowouts with a larger degree of uncertainty or lack of data in the exact blowout conditions, which is likely to be the case in immediate response or risk assessment applications. Some future work will be necessary to refine the algorithms behind the formation of non-surfacing plumes. However it may be important to note that the results may be correct in not simulating them and the possibility that the major cause of non-surfacing plumes during the Macondo Blowout may have been the use of dispersants as opposed to natural, physical processes.

In its current state, BLOSOM can handle multi-phase plumes, modeling of crude mixtures from distillate cut data; high-pressure equations-of-state for gases and crudes; hydrate formation and decomposition; some gas dissolution; transport and turbulent diffusion; and the major weathering processes of evaporation, emulsification, and dispersion. Future work will incorporate more complex hydrate models, especially for mixed-gas hydrates; increased support for gas dissolution; and more degradation processes such as dissolution, biodegradation, and photolysis. The Hydrodynamic Handler will continue to be improved to incorporate more file formats and different outputs from the plethora of ocean current models available, particularly for the nearshore where the complexity of the shorelines, estuaries, and barrier islands requires higher spatial resolution.

BLOSOM can provide comprehensive simulations of deepwater and ultra-deepwater blowout events with a relatively high-degree of accuracy both for response and risk-assessment. Its flexibility and adaptability to different inputs and conditions make it a helpful tool for risk assessment and impacts models by imparting an ability to simulate a wide variety of scenarios and providing detailed outputs for toxicity assessments. With the ever-accelerating pace to extract energy in prospect both deeper and further offshore, BLOSOM can prove a role in calculating and minimizing risks.

# REFERENCES

Adalsteinsson, D., Camassa, R., Harenberg, S., Lin, Z., Mclaughlin, R. M., Mertens, K., Reis, J., Schlieper, W., and White, B. (2011). "Subsurface Trapping of Oil Plumes in Stratification: Laboratory Investigations." *Monitoring and Modeling the Deepwater Horizon Oil Spill: A Record-Breaking Enterprise*, American Geophysical Union, Washington D.C., 257–262.

American Society of Civil Engineers. (1996). "State-of-the-Art Review of Modeling Transport and Fate of Oil Spills." *Journal of Hydraulic Engineering*, 122(11), 594–609.

Amorocho, J., and Devries, J. J. (1980). "A New Evaluation of the Wind Stress Coefficient Over Water Surfaces." *Journal of Geophysical Research*, 4, 281–310.

Atlas, R. M. (1981). "Microbial degradation of petroleum hydrocarbons: an environmental perspective." *Microbiological Reviews*, 45(1), 180–209.

Bommelé. (1985). "A Simple Computer Model for the Behavior of an Oil Spill at Sea." Rijkswaterstaat, Utrecht, NL.

Brill, J. P., and Beggs, H. D. (1973). "A Study of Two-Phase Flow in Inclinded Pipes." *Journal of Petroleum Technology*, 25(5), 607–617.

Buchanan, I. (1987). "Methods for Predicting the Physical Changes in Oil Spill at Sea." Warren Spring Laboratory, Stevenage, UK.

Camilli, R., Reddy, C. M., Yoerger, D. R., Van Mooy, B. A. S., Jakuba, M. V, Kinsey, J. C., McIntyre, C. P., Sylva, S. P., and Maloney, J. V. (2010). "Tracking Hydrocarbon Plume Transport and Biodegradation at Deepwater Horizon." *Science*, 330(201), 201–204.

Chang, A. F., Pashikanti, K., and Liu, Y. A. (2012). "Characterization , Physical and Thermodynamic Properties of Oil Fractions." *Refinery Engineering: Integrated Process Modeling and Optimization*, Wiley-VCH Verlag GmbH & Co. KGaA, Weinheim, DE.

Chen, F., and Yapa, P. D. (2004). "Modeling gas separation from a bent deepwater oil and gas jet/plume." *Journal of Marine Systems*, 45, 189–203.

Coastal Engineering Research Center. (1984). "Shore Protection Manual." U.S. Army Corps of Engineers, Washington D.C.

Deepwater Horizon Study Group. (2011). "Final Report on the Investigation of the Macondo Well Blowout." Bureau of Ocean Energy Management, Regulation, and Enforcement, Washington D.C.

Delvigne, G. A. L., and Sweeney, C. E. (1988). "Natural dispersion of oil." *Oil & Chemical Pollution*, 4, 281–310.

Elliot, A. J., Hurford, N., and J, P. C. (1986). “Shear diffusion and the spreading of oil slicks.” *Marine Pollution Bulletin*, 17, 308–313.

Englezos, P., Kalogerakis, N., Dholabhai, P. D., and Bishnoi, P. R. (1987a). “Kinetics of formation of methane and ethane gas hydrates.” *Chemical Engineering Science*, 42(11), 2647–2658.

Englezos, P., Kalogerakis, N., Dholabhai, P. D., and Bishnoi, P. R. (1987b). “Kinetics of gas hydrate formation from mixtures of methane and ethane.” *Chemical Engineering Science*, 42(11), 2659–2666.

Fanneløp, T. K., and Sjøen, K. (1980). “Hydrodynamics of Underwater Blowouts.” *Norwegian Maritime Research*, 4, 17–33.

Fay, J. A. (1971). “Physical processes in the spread of oil on a water surface.” Proc., *Joint Conference for the Prevention and Control of Oil Spills*, Washington D.C., 463–467.

Fingas, M. (2008). “A Review of Knowledge on Water-in-Oil Emulsions.” Proc., *International Oil Spill Conference*, Savannah, GA.

Fingas, M. F. (1995). “A literature review of the physics and predictive modelling of oil spill evaporation.” *Journal of Hazardous Materials*, 42(2), 157–175.

Fingas, M., and Fieldhouse, B. (2003). “Studies of the formation process of water-in-oil emulsions.” *Marine Pollution Bulletin*, 47, 369–96.

Fingas, M., and Fieldhouse, B. (2004). “Formation of water-in-oil emulsions and application to oil spill modelling.” *Journal of Hazardous Materials*, 107, 37–50.

Fisher, H. B., List, E. J., Yikoh, R. C., Imberger, J., and Brooks, N. H. (1979). *Mixing in Inland and Coastal Waters*. Academic Press, New York, NY.

Fofonoff, N. P., and Millard, R. C. (1983). “Algorithms for computation of fundamental properties of seawater.” UNESCO technical papers in marine science, Paris, FR.

Guo, B., and Ghalambor, A. (2005). *Natural Gas Engineering Handbook*. Gulf Publishing Company, Houston, TX.

Jernelöv, A., and Lindén, O. (1981). “Ixtoc I: A Case Study of the World’s Largest Oil Spill.” *Ambio*, 10(6), 299–306.

Johansen, Ø. (1984). “The Halten Bank experiment - observations and model studies of drift and fate of oil in the marine environment.” Proc., *11th Arctic Marine Oil Spill Program*, Environment Canada, Edmonton, AB.

Johansen, Ø. (2000). “DeepBlow - a Lagrangian Plume Model for Deep Water Blowouts.” *Spill Science & Technology Bulletin*, 6(2), 103–111.

Johansen, Ø. (2002). “Estimates of droplet size from subsea oil and gas leaks or blowouts.” SINTEF, Norway.

Jones, R. K. (1997). “A simplified pseudo-component oil evaporation model.” Proc., *20th Arctic and Marine Oilspill Program Technical Seminar*, Environment Canada, Emergencies Science Division, Ottawa, Canada.

Kesler, M. G., and Lee, B. I. (1976). “Improved Predicton of Enthalpy of Fractions.” *Hydrocarbon Processing*, 55(3), 153–158.

Kim, H. C., Bisnoi, P. R., Heidemann, R. A., and Rizvi, S. S. H. (1987). “Kinetics of Methane Hydrate Decomposition.” *Chemical Engineering Science*, 42(7), 1645–1653.

King, M. B. (1969). *Phase Equilibrium in Mixtures*. Pergamon, Oxford, UK.

Lee, J. H. W., and Cheung, V. (1991). “Generalized Lagrangian Model for Buoyant Jets in Currents.” *Journal of Environmental Engineering*, 116(6), 1085–1106.

Lehr, B., Aliseda, A., Bommer, P., Espina, P., Flores, O., Lasheras, J. C., Leifer, I., Possolo, A., Riley, J., Savas, O., Shaffer, F., Wereley, S., and Yapa, P. (2010). “Deepwater Horizon Release Estimate of Rate by PIV.” National Incident Command Flow Rate Technical Group, U.S. Department of the Interior, Washington D.C.

Lehr, W. J. (2001). “Review of modeling procedures for oil spill weathering behavior.” *Oil Spill Modeling and Process*, C. A. Brebbia, ed., WIT Press, Southampton, UK.

Lehr, W. J., Fraga, R. J., Belen, M. S., and Cekirge, H. M. (1984). “A new technique to estimate initial spill size using a modified Fay-type spreading formula.” *Marine Pollution Bulletin*, 15, 326–329.

MacKay, D., Paterson, S., and Trudel, K. (1980). “A mathematical model of oil spill behaviour.” Environmental Protection Service, Fisheries and Environment Canada, Ottawa, Canada.

Mackay, D., Shiu, W. Y., Hossain, K., Stiver, W., McCurdy, D., Petterson, S., and Tebeau, P. A. (1982). “Development and calibration of an oil spill behavior model.” United States Coast Guard Office of Research and Development, Groton, CT.

North, E. W., Adams, E. E., Schlag, Z., Sherwood, C. R., He, R., Hyun, K. H., and Socolofsky, S. A. (2011). “Simulating Oil Droplet Dispersal From the Deepwater Horizon Spill With a Lagrangian Approach.” *Monitoring and Modeling the Deepwater Horizon Oil Spill: A Record-Breaking Enterprise*, American Geophysical Union, Washington D.C., 217–226.

Rasmussen, D. (1985). “Oil Spill Modeling: A Tool for Cleanup Operations.” Proc., *1985 Oil Spill Conference*, Los Angeles, CA.

Reed, M., Ekrol, N., Daling, P., Johansen, Ø., Ditlevsen, M. K., Swahn, I., Resby, J. L. M., and Skognes, K. (2004). *SINTEF Oil Weathering Model User's Manual*. Trondheim, Norway.

Reed, M., Johansen, Ø., Brandvik, P. J., Daling, P., Lewis, A., Fiocco, R., Mackay, D., and Prentki, R. (1999). "Oil Spill Modeling towards the Close of the 20th Century: Overview of the State of the Art." *Spill Science & Technology Bulletin*, 5(1), 3–16.

Reinhart, R., and Rose, R. (1982). "Evaporation of Crude Oil at Sea." *Water Research*, 16, 1325–1335.

Rye, H., and Brandvik, P. J. (1997). "Verification of Subsurface Oil Spill Models." Proc., *International Oil Spill Conference*, Fort Lauderdale, Florida, 551–557.

Rye, H., Brandvik, P. J., and Reed, M. (1996). "Subsurface oil release field experiment-observations and modeling of subsurface plume behavior." Proc., *19th Arctic and Marine Oil Spill Program Technology Seminar*, Ottawa, Canada, 1417–1435.

Schatzmann, M. (1979). "Calculation of submerged thermal plumes discharged into air and water flows." Proc., *19th International Association for Hydro-Environment Engineering and Research Congress*, Delft, Netherlands, 239–246.

Sharqawy, M. H., Lienhard V, J. H., and Zubair, S. M. (2010). "Thermophysical properties of seawater: a review of existing correlations and data." *Desalination and Water Treatment*, 16, 354–380.

Shen, H. T., Yapa, P. D., and Petroski, M. E. (1987). "A Simulation Model for Oil Slick Transport in Lakes." *Water Resources Research*, 23(10), 1949–1957.

Sloan, E. D. (1997). *Clathrate Hydrates of Natural Gases*. 2nd Ed., Marcel Dekker, New York, NY.

Smagorinsky, J. (1963). "General circulation experiments with the primitive equations I. The basic experiment." *Monthly Weather Review*, 91, 99–164.

Walker, J. D., Colwell, R. R., and Petrakis, L. (1976). "Biodegradation rates of components of petroleum." *Canadian Journal of Microbiology*, 22(8), 1209–13.

Wang, S., Shen, Y. M., and Zheng, Y. (2005). "Two-dimensional numerical simulation for transport and fate of oil spills in seas." *Ocean Engineering*, 32, 1556–1571.

Yapa, P. D., and Zheng, L. (1997). "Simulation of Oil Spills From Underwater Accidents I: Model Development." *Journal of Hydraulic Research*, 35(5), 673–687.

Yapa, P. D., Zheng, L., and Chen, F. (2001). "A Model for Deepwater Oil/Gas Blowouts." *Marine Pollution Bulletin*, 43, 234–241.

Zheng, L., and Yapa, P. D. (2000). “Buoyant Velocity of Spherical and Nonspherical Bubbles/Droplets.” *Journal of Hydraulic Engineering*, 126(11), 852–854.

Zheng, L., and Yapa, P. D. (2002). “Modeling gas dissolution in deepwater oil/gas spills.” *Journal of Marine Systems*, 31(4), 299–309.

Zheng, L., Yapa, P. D., and Chen, F. (2002). “A model for simulating deepwater oil and gas blowouts – Part I: Theory and model formulation.” *Journal of Hydraulic Research*, 41(4), 339–351.